Title page

Manuscript title

Prdm1 Positively Regulates Liver Group 1 ILCs Cancer Immune Surveillance and Preserves Functional Heterogeneity

Authors and affiliations

Jitian He[1], Le Gao[1], Peiying Wang[1], Wing Keung Chan[4], Yiran Zheng[1], Yumo Zhang[1], Jiaman Sun[1], Xue Li[8], Jiming Wang[5], Xiaohong Li[1], Huaiyong Chen[3,6,7], Zhouxin Yang[2], Youwei Wang[1]

[1]Institute of Medical Engineering & Translational Medicine, Tianjin University, Tianjin 300072, China.

[2]Zhejiang Provincial Key Lab of Geriatrics and Geriatrics Institute of Zhejiang Province, Zhejiang Hospital, Hangzhou 310030, China.

[3]College of Pulmonary and Critical Care Medicine, 8th Medical Center, Chinese PLA General Hospital, Beijing, China.

[4]Department of Internal Medicine, Division of Hematology, The Ohio State University, Columbus, OH 43210, USA.

[5]Tianjin Economic-Technological Development Area (TEDA) Hospital, Tianjin 300451, China.

[6]Department of Basic Medicine, Haihe Hospital, Tianjin University, Tianjin 300350, China.

[7]Tianjin Key Laboratory of Lung Regenerative Medicine, Tianjin 300350, China.

[8]Department of Basic Medicine, Haihe Hospital, Tianjin University, Tianjin 300350, China

Authorship notes: JH, LG, and PW contributed equally to this work.

Co-corresponding authors: Xiaohong Li (xhli18@tju.edu.cn), Huaiyong Chen (huaiyong.chen@foxmail.com), Zhouxin Yang (yangzhouxin@hotmail.com), and Youwei Wang (youwei.wang@tju.edu.cn)

Address correspondence to: Youwei Wang, Institute of Medical Engineering & Translational Medicine, Tianjin University, Tianjin 300072, China. Email: youwei.wang@tju.edu.cn. Or to Zhouxin Yang, Zhejiang Provincial Key Lab of Geriatrics and Geriatrics Institute of Zhejiang Province, Zhejiang Hospital, Hangzhou 310030, China. Email: yangzhouxin@hotmail.com. Or to Huaiyong Chen, Department of Basic Medicine, Haihe Hospital, Tianjin University, Tianjin 300350, China. Email: huaiyong.chen@foxmail.com.

Abstract

Group 1 innate lymphoid cells (ILCs) comprise conventional natural killer (cNK) cells and type 1 innate lymphoid cells (ILC1s). The main functions of liver cNK cells and ILC1s not only include directly killing target cells but also regulating local immune microenvironment of the liver through the secretion of cytokines. Uncovering the intricate mechanisms by which transcriptional factors regulate and influence the functions of liver cNK cells and ILC1s, particularly within the context of liver tumors, presents a significant opportunity to amplify the effectiveness of immunotherapies against liver malignancies. Using Ncr1-drived conditional knockout mouse model, our study reveals the regulatory role of *Prdm1* in shaping the composition and maturation of cNK cells. Although *Prdm1* did not affect the killing function of cNK cells in an *in vivo* cytotoxicity model, a significant increase in cancer metastasis was observed in *Prdm1* knockout mice. Interferon-gamma (IFN-γ), granzyme B, and perforin secretion decreased significantly in *Prdm1* deficient cNK cells and liver ILC1s. scRNA sequencing data also provided evidences that Prdm1 maintains functional subsets of cNK cells and liver ILC1s and facilitates communications between cNK cells, liver ILC1s and macrophages. The present study unveiled a novel regulatory mechanism of Prdm1 in cNK cells and liver ILC1s, showing promising potential for developing innovative immune therapy strategies against liver cancer.

Main text

Introduction

Group 1 ILCs consist of cNK cells and ILC1s (1, 2), with distinct developmental trajectories and effect molecules (3). Both cNK cells and ILC1s play indispensable roles in combatting viral infections (4), maintaining local immune homeostasis (5), eradicating malignant transformed cells (6), and fostering cross-talk with adaptive immunity (7). cNK cells demonstrate potent cellular cytotoxicity, facilitating direct elimination of target cells (8). On the contrary, a defining attribute of ILC1s is their predominant cytokine-mediated functions, with limited cellular killing capacity (9). In a state of homeostasis, liver group 1 ILCs ($CD45^{+}CD3^{-}NK1.1^{+}NKp46^{+}$) can be discriminated into cNK cells and ILC1s by the differential expression of CD49a and CD49b (2): cNK cells are marked by the expression of CD49b, while liver ILC1s exhibit a distinctive positivity for CD49a. Tumor Necrosis Factor Related Apoptosis Inducing Ligand (TRAIL) is also expressed on liver ILC1s, but not on cNK cells (10). Transcriptional factors (TFs) such as T-bet, Nfil3, PLZF, and ID2 are required for cNK cells and liver ILC1s development or generation of their progenitors (11-14). Eomes is considered to be necessary for NK cell maturation, but not for ILC1s (15). Liver environment facilitated T-bet expression in the early stage of NK cells development, which results in Eomes repression. The repression of T-bet is required for $Eomes^{+}$ NK cells (16). On the contrary, deficiency of Hobit results in the depletion of ILC1s, while only leaving little impact on liver NK cells (17). These studies suggest that some TFs may, or usually, play different roles in NK cells and ILC1s.

During the development of liver cancers, the functions of immune cells are often inhibited,

resulting in the formation of an immunosuppressive tumor microenvironment, and sometimes even systemic immune suppression (18). Transforming a cold tumor into a hot tumor with a stronger immune response is one of the goals of many cancer immunotherapies (19). Research targeting the immune system is showing increasing clinical promise in liver cancer treatment (20). One of our recent studies also found that Toll-like receptor agonists can significantly enhance the anti-tumor effect of Sorafenib by reconstructing the tumor immune microenvironment and reshaping the vascular system (21).

The anti-tumor activity of cNK cells in the liver is relatively well-established, whereas the relationship between liver ILC1 and tumors is still a topic of controversy. Clinical data showed that liver tumors with a higher infiltration of NK cells are associated with a better prognosis (22). Decreased NK cell activity is closely correlated with the malignancy of liver tumors and represents a significant risk factor for recurrence (23). The tumor microenvironment orchestrates the transformation of cNK cells into ILC1s in a TGF-β-dependent manner, resulting in their diminished capacity to control tumor growth and metastasis. This process ultimately promotes tumor immunoevasion (24). However, researches also revealed that, distinct from directly inhibiting tumor growth, the primary function of ILC1 is to suppress the seeding of metastatic tumor cells in liver tissue (6). Comprehensive research in this field is essential to harness the precision of group 1 ILCs targeted immunotherapy for liver cancers.

The transcription factor network governs the function of group 1 ILCs and the balance between cNK and ILC1. Our research team, along with others, has observed that one of the transcription factor in TGF-β pathway, Smad4, promotes the shift in balance from cNK cells towards ILC1 in a TGF-beta-independent pathway, and simultaneously, it positively regulates the

expression of another transcription factor, PR domain 1 (Prdm1/Blimp1) (25, 26). Prdm1 plays a crucial role in the differentiation of B cells into plasma cells and the homeostasis of T cells (27-29). The function and regulatory network of Prdm1 in NK cells is distinct from B cells and T cells, for its expression is independent of B-cell lymphoma 6 (Bcl-6) and Interferon Regulatory actor 4 (IRF4) but relies on T-bet. In the study that identified Prdm1 as an essential transcriptional factor for NK cell maturation (30), no significant differences were observed in IFN-γ production or cytotoxicity between Prdm1-deficient and wild-type NK cells. Although Prdm1 expression is dependent on IL-15 in immature NK cells and can be further upregulated by IL-12 or IL-21, it plays a role in downregulating the expression of certain cytokine receptors, such as CD25, consequently diminishing the responsiveness of NK cells to IL-2 (31). Notably, some studies even suggested that Prdm1 suppressed the secretion of IFN-γ in NK cells (32). These findings imply that, although Prdm1 promotes NK cell development, it may function as a negative regulator of their activity. However, direct evidence supporting the impact of Prdm1 on NK cell anti-tumor capabilities is still lacking. Furthermore, there has been no investigation into its influence on the homeostasis of cNK cells and ILC1s in the liver, nor has there been an exploration of the underlying mechanisms.

In the current study, we found that the deletion of *Prdm1* in Ncr1^{+} cells resulted in an imbalance in the homeostasis of liver group 1 ILCs, with a shift towards cNK cells. The data also support the essential role of Prdm1 in the cancer surveillance mediated by cNK cells. While Prdm1 positively regulates genes associated with cellular cytotoxicity, it concurrently exerts inhibitory control over certain positive regulators of NK cell development and functionality, such as JunB. Using single-cell RNA sequencing, we have identified a subset of cNK cells within the

liver characterized by elevated JunB expression. These cells exhibit decreased expression of genes associated with cellular cytotoxicity, and their abundance significantly increases following Prdm1 knockout. Furthermore, our data also support that Prdm1 promotes the cross-talk between group 1 ILCs and macrophages.

Results

Prdm1 promotes group 1 ILCs homeostasis and terminal maturation

Examination of 363 liver hepatocellular carcinoma (LIHC) patient samples from The Cancer Genome Atlas (TCGA) revealed a positive correlation between the expression of NK cell-associated genes (33) (*NCR1*, *KLRB1*, *CD160*, *PRF1*, etc.) and *PRDM1* expression (Figure 1A). The patients are ordered from highest to lowest based on the expression of NK-PRDM1 for survival analysis (Figure 1B). Notably, patients exhibiting higher levels of NK-PRDM1 expression (above the median) experienced better survival outcomes compared to those with lower levels of NK-PRDM1 expression (below the median) (Figure 1C). Similar results were also found in skin cutaneous melanoma (SKCM, n=454) and lung adenocarcinoma (LUAD, n=497) patients (Figure 1—figure supplement 1, A-F). Patients within the highest quartile of NK-PRDM1 signature expression demonstrated enhanced overall survival, a result that achieved statistical significance in LUAD and SKCM patients (Figure 1—figure supplement 1, G-I). These data suggested that *PRDM1* in NK cells might be essential for immune surveillance in solid tumors, including liver cancer, and prompted us to investigate the function and mechanism of *PRDM1* in NK cells and ILC1 within the context of liver cancer.

Ncr1-Cre mice were crossed with *Prdm1*$^{fl/fl}$ mice to generate *Ncr1-cre Prdm1*$^{fl/fl}$ mice, which

specifically knockout exons 6-8 of *Prdm1* (34) in NKp46 positive cells (Figure 1D). The mice carrying *Ncr1*$^{Cre/+}$*Prdm1*$^{fl/fl}$ were referred to as *Prdm1*$^{\Delta Ncr1}$ mice, and the mice carrying *Ncr1*$^{+/+}$*Prdm1*$^{fl/fl}$ were referred to as *Prdm1*$^{+/+}$ mice or wild-type (WT) mice. To further validate the deletion of *Prdm1* in NKp46^{+} cells of *Prdm1*$^{\Delta Ncr1}$ mice, CD3^{-}NK1.1^{+}NKp46^{+} cells were sorted and the expression of *Prdm1* was measured by real-time RT-PCR. The expression of *Prdm1* was almost undetectable in CD3^{-}NK1.1^{+}NKp46^{+} cells of *Prdm1*$^{\Delta Ncr1}$ mice, while was similar between total splenocytes in *Prdm1*$^{+/+}$ and *Prdm1*$^{\Delta Ncr1}$mice (Figure 1, E and F**)** indicating successful, and specifical knockout of *Prdm1* in NKp46^{+} cells.

Proportion and absolute number of NK cells in blood, bone marrow, lung, liver, spleen, and lymph nodes were analyzed by flow cytometry. Compared with *Prdm1*$^{+/+}$ mice, the percentage and absolute number of NK cells (CD45^{+}CD3^{-}NK1.1^{+}NKp46^{+}) among lymphocytes was decreased in all of these tissues, whereas increased number of NK cells were observed in bone marrow (Figure 1G; Figure 1—figure supplement 2A). NK cell terminal maturation can be divided into four stages according to the expression of CD11b and CD27 (35). Stage IV (CD11b^{+}CD27^{-}) NK cells show higher level of effector molecules than any other stages and are considered as the most mature NK cells (36). The maturation of cNK cells (gated by CD45^{+}CD3^{-}NK1.1^{+}NKp46^{+}CD49b^{+}) from blood, bone marrow, lung, liver, spleen, and lymph nodes were assessed, based on the expression of CD11b and CD27. Compared with *Prdm1*$^{+/+}$ mice, the proportion of the most mature CD11b^{+}CD27^{-} NK cells were significantly decreased in all of the analyzed tissues in *Prdm1*$^{\Delta Ncr1}$ mice (Figure 1H; Figure 1—figure supplement 2B). Killer cell lectin-like receptor subfamily G member 1 (KLRG1) is a lectin-like receptor which was considered as another marker of NK cell maturation (37). In both *Prdm1*$^{+/+}$ and *Prdm1*$^{\Delta Ncr1}$ mice,

NK cells from the liver and lung had the highest expression of KLRG1, following by blood and spleen (Figure 1—figure supplement 2C). The lowest KLRG1 expression was observed in NK cells derived from lymph nodes and bone marrow, indicating the presence of the most immature NK cells in these tissues. Consistent with CD11b/CD27 based maturation analysis, a significant loss of KLRG1^{+} cells in NK cells was observed in *Prdm1*$^{\Delta Ncr1}$ mice (Figure 1—figure supplement 2C). Together, these data confirmed that *Prdm1* is required for the terminal maturation of NK cells among various tissues.

Prdm1 is required for group 1 ILCs to control tumor metastasis

Two subpopulations of liver group 1 ILCs (gated by CD45^{+}CD3^{-}NK1.1^{+}NKp46^{+}) were further analyzed based on the expression of CD49a and CD49b (Figure 2A). Compared with *Prdm1*$^{+/+}$ mice, the *Prdm1*$^{\Delta Ncr1}$ mice exhibited an increased percentage of cNK cells (CD49a^{-}CD49b^{+}) and reduced proportion of ILC1s (CD49a^{+}CD49b^{-}) (Figure 2A). Of note, the absolute number of both cNK cells and ILC1s were decreased in *Prdm1*$^{\Delta Ncr1}$ mice, with a more robustly reduction in ILC1s (Figure 2A), which underscored the crucial role of *Prdm1* in maintaining the quantity of both liver cNK cells and ILC1s. Expression level of CD49b was slightly upregulated in *Prdm1*$^{\Delta Ncr1}$ cNK cells and NKp46^{+} cells in the liver and other tissues (Figure 1—figure supplement 2, D and E). Increased CD49a expression was also observed in *Prdm1*$^{\Delta Ncr1}$ liver ILC1s, while it showed decreased expression in NKp46^{+} cells in the liver, bone marrow, and lymph nodes (Figure 1—figure supplement 2, F and G). These results indicated the essential role of Prdm1 in maintaining the balance and hemostasis of cNK cells and ILC1s.

The decreased quantity of NK cell homeostasis and maturation of cNK cells due to *Prdm1*

loss motivated us to further explore whether deficiency of Prdm1 impaired NK cell cytotoxicity. A B2M-deficient cell-based *in vivo* cytotoxicity assay was used to evaluate the effect of *Prdm1* on the cytotoxicity of NK cells (38, 39). B2M-deficient cells do not have detectable Major Histocompatibility Complex I (MHC-□) on the cell surface, making them the target of NK cells (40). Healthy NK cells will reject B2M-deficient donor cells efficiently and the elimination was used to quantify the cytotoxicity of NK cells. Although significant impaired homeostasis and maturation of NK cells were observed in *Prdm1*$^{\Delta Ncr1}$ mice, no significant difference in the *in vivo* cytotoxicity assay were observed between *Prdm1*$^{+/+}$ and *Prdm1*$^{\Delta Ncr1}$ mice (Figure 1—figure supplement 2, H and I).

Besides their direct cytotoxic capabilities, NK cells' anti-tumor potential is also influenced by additional factors. These include their ability to counteract tumor-induced immune suppression and exhaustion, enhancing their effectiveness against cancer cells. Furthermore, NK cells can secrete cytokines that activate other immune cells, thereby orchestrating a broader immune response for the elimination of tumors. Moreover, the cytotoxicity assay, due to its relatively short duration, might not fully represent the anti-tumor activity of NK cells when continuously exposed to immune inhibitory signals in the tumor microenvironment. Therefore, we initiated an *in vivo* tumor model to further investigate the impact of *Prdm1* on NK cell anti-tumor capability. B16F10 is a melanoma cell line with low expression of MHC-□, which was susceptible to NK cell killing and usually used to evaluate NK cell anti-tumor capacity (41-43). The B16F10 cells were intravenously (for lung metastasis) or intrasplenic (for liver metastasis) administrated in the mice. The melanoma nodes were quantified three (intravenous injection) or two (intrasplenic injection) weeks after tumor inoculation. Compared with *Prdm1*$^{+/+}$ mice, deficiency of *Prdm1* resulted in

more metastasis nodules in both lung (~ 2-fold) and liver (~ 4-fold) (Figure 2, B and D). Histological analysis further confirmed the increased frequency of metastasis tumor foci in *Prdm1*$^{\Delta Ncr1}$ mice (Figure 2, C and E).

In agreement with our *in vivo* data, we also observed decreased IFN-γ secretion in *Prdm1*$^{\Delta Ncr1}$ mice-derived splenic cNK cells, liver cNK cells, and liver ILC1s when stimulated by IL-18 alone or IL-12/IL-18 (Figure 2F; Figure 2—figure supplement 1; Figure 7—figure supplement 1B), which indicated that *Prdm1* is required for full activation of cNK cells and ILC1s in the context of IFN-γ production. These data implied that *Prdm1* is indispensable for NK cell mediated tumor surveillance.

Bulk RNA-seq depicts *Prdm1*-mediated functions in cNK cells

Bulk RNA sequencing of splenic cNK cells (CD3$^-$NK1.1$^+$NKp46$^+$) was conducted to uncover the molecular mechanisms by which *Prdm1* regulates NK cell anti-tumor immunity (Figure 3A). Differentially expressed genes (DEGs) between *Prdm1*$^{+/+}$ and *Prdm1*$^{\Delta Ncr1}$ mice were determined using a criterion of $\log_2$(fold change) > 0.5 and $P < 0.05$. 445 DEGs were identified out of 17434 protein-coding genes, which consisted of 223 upregulated genes and 222 downregulated genes (Figure 3B).

Gene Ontology (GO) analysis revealed the enrichment of glucuronate metabolism and lymphocyte differentiation in upregulated genes in *Prdm1*$^{\Delta Ncr1}$ mice derived NK cells (Figure 3C), both of which were associated with cellular growth and development. In contrast, leukocyte mediated cytotoxicity, immune receptor activity, and integrin binding were enriched in the genes which decreased their expression level in in *Prdm1*$^{\Delta Ncr1}$ mice (Figure 3C). Gene Set Enrichment

Analysis (GSEA) showed that NF-kappa B signaling pathway enriched in *Prdm1*-deficient cNK cells (Figure 3D), suggesting the potential targets by *Prdm1* to regulate NK cell function. Increased expression of multiple TFs such as *Junb*, *Batf3*, *Nfkb1*, *Tcf7*, and *Nr4a2* was observed in *Prdm1* knockout cNK cells, suggesting they might be suppressed by *Prdm1* (Figure 3E). Downregulation of granzyme B (*Gzmb*), Perforin (*Prf1*) were observed in *Prdm1* deficient NK cells (Figure 3E), implying decreased anti-tumor ability, which was consistent with increased melanoma metastasis in *Prdm1*$^{\Delta Ncr1}$ mice (Figure 2, B and D). CXCR6 and CX3CR1 was considered to play an important role in promoting the egress of NK cells from bone marrow. Decreased expression of *Cxcr6* and *Cx3cr1* in *Prdm1*$^{\Delta Ncr1}$ NK (Figure 3E) might be the reason for the increased quantity of NK cells in bone marrow and decreased number in peripheral tissues (Figure 1G). As a result of the reduced expression levels of *Cxcr6* and *Cx3cr1*, NK cells may not be able to egress from the bone marrow and accumulated therein. Consistent with decreased production of IFN-γ after stimulated by IL-12/IL-18 (Figure 2F), decreased expression of *Il18rap* and *Il12rb2* were observed in *Prdm1*$^{\Delta Ncr1}$ cNK cells (Figure 3E), implying impaired response to cytokine stimulation.

To confirm the result of RNA-sequencing, the expression of fractalkine receptor (CX3CR1), granzyme B and perforin were analyzed by flow cytometry. The percentage of CX3CR1^{+} cNK cells was significantly decreased in multiple tissues of *Prdm1*$^{\Delta Ncr1}$ mice, while the proportion of CX3CR1^{+} ILC1 was increased in the liver (Figure 3, F and G). Lower GZMB and PRF1 production was observed in *Prdm1*-deficient splenic cNK cells, liver cNK cells and ILC1s (Figure 3, H-K; Figure 3—figure supplement 1, A-I). Notably, the proportion of GZMB^{+} and PRF1^{+} cNK cells was decreased among almost all of the maturation stages of cNK cells (Figure 3, J and K).

The relative mean fluorescent intensities (MFIs) of GZMB and PRF1 consistently show a reduction across all developmental stages in *Prdm*$^{\Delta Ncr1}$ NK cells (Figure 3—figure supplement 1, H and I). Yet, no statistical difference of PRF1 was found within the CD11b^{-}CD27^{+} and CD11b^{+}CD27^{+} subsets, likely due to the relatively lower perforin levels in these populations (Figure 3—figure supplement 1I). These findings suggest that Prdm1 may directly influence cytotoxic molecule in NK cells, rather than impacting their anti-tumor abilities solely by affecting the maturation phenotype of Prdm1-deficient NK cells.

scRNA-seq reveals distinct properties of two clusters from liver group I ILCs following *Prdm1* knockout

To further investigate the effect of *Prdm1* in liver cNK cells and ILC1s and the changes in the hepatic immune microenvironment caused by the deficiency of *Prdm1* in group 1 ILCs, single-cell RNA sequencing (scRNA-seq) was performed for liver CD45^{+} cells (Figure 4A; Figure 4—figure supplement 1A). Initial quality control revealed high-quality of cell purity, library assembly, and sequencing (Figure 4—figure supplement 1B). 10,978 cells passed the quality criteria and were selected for further analysis (6,161 from *Prdm1*$^{+/+}$ mice, 4,817 from *Prdm1*$^{\Delta Ncr1}$ mice). Unsupervised clustering of all sequenced cells based on transcript signatures identified twelve distinct clusters (Figure 4—figure supplement 1C), including B cells, epithelial cells (ECs), CD4^{+} T cells, CD8^{+} T cells, NKT cells, ILC1s, cNK cells, dendritic cells (DCs), monocyte-derived macrophages (MDMs), Monocytes, Kupffer cells (KCs), Neutrophils, and a small number of undefined cells (Figure 4A). In *Prdm1*$^{\Delta Ncr1}$ mice, an increased proportion of MDMs, CD4^{+} T cells, CD8^{+} T cells, Monocytes, and DCs was observed, alongside a decreased proportion of ECs, cNK

cells, ILC1s, and NKT cells (Figure 4—figure supplement 1D). Liver cNK cells and ILC1s were identified and discriminated based on the expression of surface markers and distinctive TFs (Figure 4—figure supplement 1, E and F). Compared with other clusters, cNK cells and ILC1s highly expressed *Ncr1* and *Klrb1c* (NK1.1) (Figure 4—figure supplement 1E). cNK cells expressed high levels of *Itga2* (CD49b) and Eomes, while ILC1s had high levels expression of *Itga1* (CD49a) and *Tnfsf10* (Figure 4—figure supplement 1, F and G). Consistent with our flow cytometry data, both cNK cells and ILC1s have significant reduced proportion in *Prdm1*$^{\Delta Ncr1}$ mouse (Figure 4—figure supplement 1H). In group 1 ILCs from *Prdm1*$^{\Delta Ncr1}$ mice, there was an increase in the proportion of cNK cells accompanied by a decrease in ILC1s (Figure 4, B and C).

To better understand the specific function of *Prdm1* in liver cNK cells and ILC1s, the two subpopulations of liver group 1 ILCs were further analyzed separately using unsupervised clustering and visualized by Uniform Manifold Approximation and Projection (UMAP) (Figure 4, D and E). Based on the cluster specific gene expression signature (Figure 4—figure supplement 2A), the subpopulation of liver cNK cells were referred as "*Prf1*^{hi}", "*Junb*^{hi}", and "*Cxcr3*^{hi}" cNK cells (Figure 4D), with different distribution in *Prdm1*$^{\Delta Ncr1}$ and *Prdm1*$^{+/+}$ genotype (Figure 4F; Figure 4—figure supplement 2B).

The *Prf1*^{hi} cNK cell cluster was defined by high expression of cytolysis-related genes, including *Ncr1*, *Gzma*, *Gzmb*, *Prf1*, and *Fgl2* (Figure 4G; Figure 4—figure supplement 2, C and D), indicating the strong target-killing ability of this cluster. Although this cluster is present in both *Prdm1*$^{\Delta Ncr1}$ and *Prdm1*$^{+/+}$ mice, there is a significant reduction in *Prdm1*$^{\Delta Ncr1}$ mice (Figure 4F), indicating the importance of Prdm1 in maintaining this group of cells. GO analysis further revealed the enrichment signatures of cytolysis, response to virus, and lymphocyte mediated

immunity in the genes upregulated in *Prf1*^{hi} cNK cell cluster, further confirming the cytotoxic effects of this cluster (Figure 4H). These data underscore the crucial role of *Prdm1* in maintaining NK cells with immune effector functions.

The *Junb*^{hi} liver cNK cell cluster distinguished themselves by higher expression of *Junb* compared to other clusters (Figure 4G; Figure 4—figure supplement 2, C and D). The predominant majority (92.98%) of *Junb*^{hi} liver cNK cells are derived from *Prdm1*$^{\Delta Ncr1}$ mice, with less than ten percent (7.02%) originating from *Prdm1*$^{+/+}$ mice (Figure 4F). Many signal transduction elements, gene expression regulator, and transcriptional factors, such as *Nfkbia*, *Tnfaip3*, *Nr4a1/2/3*, *Batf3*, *Fos*, *Fosb*, *Tcf7*, and *Kit* were upregulated in the *Junb*^{hi} liver cNK cells (Figure 4G; Figure 4—figure supplement 2D). The expression of cytotoxicity related genes, such as *Gzmb* and *Prf1*, in *Junb*^{hi} cluster was also lower than other cNK cell clusters (Figure 4G). GO analysis showed that the genes upregulated in *Junb*^{hi} liver cNK cells enriched in cell differentiation, cell activation, and transcriptional regulation (Figure 4H). GSEA indicates that the NF-kappa B, IL-17, MAPK, and TNF signaling pathways were upregulated in this clusters (Figure 4, I-L). GSEA also showed that mitochondrial related pathways, such as mitochondrial protein, oxidative phosphorylation, and respiratory electron transport chain were suppressed in *Junb*^{hi} cNK cell cluster (Figure 4—figure supplement 2, E-G). Increased proportion of *Junb*^{hi} cluster in *Prdm1* deficient cNK cells suggested impaired anti-tumor activity, which was consistent with more melanoma metastasis in *Prdm1*$^{\Delta Ncr1}$ mice and lower expression of cytotoxicity-related genes in splenic cNK cells based on bulk RNA-sequencing.

The *Cxcr3*^{hi} cNK cell cluster was characterized with high expression of *Cxcr3*, *Ccr2*, and some genes encoding ribosomal subunits such as *Rps7* (Figure 4—figure supplement 2A).

Expression of tissue-resident markers Cd69 was also highly expressed in this clusters (Figure 4—figure supplement 2D). The enrichment of chemokine receptors in the genes upregulated in the *Cxcr3*^{hi} cluster implied a greater likelihood of this cluster being tissue-resident compared with other cNK cell clusters (Figure 4H). To further confirmed tissue-resident properties of this clusters, we calculated the module score based on top30 DEGs in ILC1 versus cNK clusters, including *Cxcr6*, *Itga1*, *Cd160*, *Cd226*, etc. *Cxcr3*^{hi} cNK clusters have the highest score among all cNK clusters (Figure 4—figure supplement 2H), indicating the similarity with liver ILC1s. In the tumor microenvironment, reports indicated that NK cells could transform into ILC1s (24). If this conversion of cNK cells into ILC1s also occurred under normal physiological conditions, then *Cxcr3*^{hi} cNK cell cluster might be the most susceptible to such transformation.

The significant enrichment of ribosomal subunits and cytoplasmic translation in *Cxcr3*^{hi} cluster (Figure 4H) implied their distinct and active metabolic profile and the capability to mount immune responses. The remarkably decreased proportion of *Cxcr3*^{hi} cNK cell cluster in *Prdm1*$^{\Delta Ncr1}$ mice (Figure 4F) emphasized the critical role of *Prdm1* in maintaining this cluster of liver cNK cells, consistent with the flow cytometry result that showed an increase in the number of NK cells in the bone marrow and a decrease in NK cells in peripheral tissues (Figure 1G). To confirm the regulatory effect of Prdm1 on the migration of NK cells and ILC1 through chemokine receptors, and to validate the scRNA-seq data, we further evaluated the expression of CX3CR1 by flow cytometry. A decrease in the proportion of CX3CR1^{+} NK cells was observed across all tested organs following Prdm1 knockout. However, it is noteworthy that, in contrast to the trend in NK cells, CX3CR1 expression was increased in liver ILC1s after Prdm1 knockout (Figure 3, F and G). This not only substantiates the involvement of Prdm1 in managing NK cell migration but also

underscores its distinctive regulatory impacts on the chemokine receptor expressions within NK cells and ILC1 populations. Bulk RNA sequencing data also found that the expression of *Cx3cr1* and *Cxcr6* decreased in *Prdm1*$^{\Delta Ncr1}$ cNK cells (Figure 3E). These findings supported the hypothesis that *Prdm1*, through regulating chemokine receptor expression levels, influenced the distribution of NK cells in the bone marrow and peripheral tissues, particularly within the liver tissue.

Three clusters of ILC1s were identified from liver ILC1s (Figure 5A), comprising "*Il7r*^{hi}", "*Klra*^{hi}", and "*Gzmb*^{hi}" ILC1s. *Prdm1*$^{+/+}$ and *Prdm1*$^{\Delta Ncr1}$ ILC1s seemed to co-cluster largely and have minor difference within the proportion of clusters (Figure 5, B and C; Figure 5—figure supplement 1B). The first two clusters of ILC1s were characterized by higher expression of *Il7r* (CD127) and *Klra5* separately, while the *Gzmb*^{hi} ILC1 cluster was identified by elevated expression of both *Gzma* and *Gzmb* (Figure 5D; Figure 5—figure supplement 1, A, C and D). Additionally, both *Gzma* and *Gzmb* expression were downregulated, and *Junb* was upregulated, in *Prdm1*$^{\Delta Ncr1}$ mice derived cNK cells and ILC1s compared to those from *Prdm1*$^{+/+}$ mice (Figure 5E). The *Il7r*^{hi} ILC1s cluster was distinguishable from other ILC1 clusters by its high expression of *Il7r*, IL18RA (*Il18r1*), and IFN-γ (*Ifng*) (Figure 5B; Figure 5—figure supplement 1C). The high expression of *Il18r1* and *Ifng* in *Il7r*^{hi} ILC1s indicated this cluster of cells was highly responsive to IL-18 (Figure 5—figure supplement 1D). GSEA and GO analysis showed that IL-17, NF-kappa B, TNF, MAPK signaling pathway and T cell differentiation were activated in the *Il7r*^{hi} ILC1 cluster (Figure 5, F-H; Figure 5—figure supplement 1, E-G). Module scores, calculated based on the expression of feature genes within the *Junb*^{hi} cNK cell cluster, revealed a comparable *Junb*^{hi} signature expression pattern within the *Il7r*^{hi} ILC1 cluster (Figure 5I). Several ILC3 signature

genes, such as *Rora*, *Tmem176a*, and *Tmem176b* (44), highly expressed in this cluster (Figure 5—figure supplement 1D). Considering the close relationship between IL-17 mediated immunity response and ILC3 (1, 45), it is plausible that *Il7r*^{hi} ILC1 cluster may be attributed, at least in part, to potential plasticity between ILC1 and ILC3 subsets.

The second liver ILC1 cluster, characterized by high expression of Ly49E (*Klra5*) and Ly49G (*Klra7*), was designated as the *Klra*^{hi} ILC1 cluster (Figure 5D; Figure 5—figure supplement 1D). Notably, there was an elevated proportion of *Klra*^{hi} ILC1s in *Prdm1*$^{\Delta Ncr1}$ ILC1s (39.7%) compared to *Prdm1*$^{+/+}$ ILC1s (28.1%) (Figure 5C). Liver Ly49E^{+} ILC1s have been identified as possessing greater cytotoxic potential and a more robust viral response compared to liver Ly49E^{-} ILC1s (46). The *Klra*^{hi} cluster exhibited notably high expression of *Ccl5* (Figure 5—figure supplement 1D). Previous research has underscored the pivotal role of CCL5, produced by both cNK cells and ILC1s, in facilitating the accumulation of DCs within the tumor microenvironment, thereby impeding tumor immune evasion, as highlighted in studies (47, 48). The expression of *Ccl5* was reduced in the *Klra*^{hi} cluster of *Prdm1*$^{\Delta Ncr1}$ ILC1s compared to *Prdm1*$^{+/+}$ ILC1s (Figure 5—figure supplement 1D), which could potentially have a detrimental impact on the ability of *Klra*^{hi} ILC1s to develop a connection between innate and adaptive immune responses.

The *Gzmb*^{hi} ILC1 cluster was identified according to the high expression of *Gzma*, *Gzmb*, and *Fgl2* (Figure 5—figure supplement 1D) compared to other ILC1 clusters. GO analysis also revealed the enrichment in cytolysis and stimulus-response capacity (Figure 5H) of the *Gzmb*^{hi} ILC1 cluster. Consistent with the *Prf1*^{hi} cNK cell cluster, the proportion of the *Gzmb*^{hi} cluster among liver ILC1s exhibited a considerable reduction in *Prdm1*$^{\Delta Ncr1}$ mice compared to *Prdm1*$^{+/+}$ mice, and the expression of *Gzma* also downregulated in *Prdm1*$^{\Delta Ncr1}$ mice (Figure 5B). Previous

reports showed that GzmA^{+} ILC1 constituted the main population of liver ILC1s at birth, with the potential target-killing ability (49, 50). Within cNK cells, *Il12rb2*, *Il18r1* and *Il18rap* was highly expressed in *Prf1*^{hi} and *Cxcr3*^{hi} cNK clusters (Figure 4—figure supplement 2I), indicating the IL-18 receptor expression correlated with the NK cell maturation. While in ILC1, these receptors mostly expressed on *Il7r*^{hi} and *Gzmb*^{hi} ILC1 clusters (Figure 5—figure supplement 1D). Significant decreased of *Il18r1* expression in *Prdm1*$^{\Delta Ncr1}$ cNK cells and ILC1s may associated with the impaired ability to produce IFN-γ.

To investigate the universal transcriptional program between group 1 ILCs across liver and spleen, we have explored DEGs in *Prdm1*$^{\Delta Ncr1}$ liver cNK cells and ILC1s using our scRNA-seq data. Compared with liver ILC1s, more valuable DEGs was observed in liver cNK cells, including *Junb*, *Kit*, *Tcf7*, *Gzmb*, *Prf1*, etc. (Figure 5—figure supplement 2, A and B). Through the integration of the bulk RNA-seq and scRNA-seq data, we identified 17 DEGs that are regulated by Prdm1 among liver cNK cells, splenic cNK cells, and liver ILC1s. *Batf3*, *Junb*, *Tcf7*, and *Nfkb1* was upregulated, whereas *Gzmb*, *Prf1*, and *Fgl2* downregulated, in both *Prdm1*$^{\Delta Ncr1}$ liver and splenic cNK cells (Figure 5J). Cxcr6 was downregulated in liver ILC1s and splenic cNK cells in *Prdm1*$^{\Delta Ncr1}$ mice (Figure 5J). Previous research found that spleen NK cells could be divided into three distinct groups based on their expression levels of CD27, CD62L, CD49a, and CD49b (51). CD27^{+}CD62L^{-} NK cells have remarkable high expression of Batf3, while it was only barely expressed in CD27^{+}CD62L^{+} and CD27^{-}CD62L^{+} NK cells (51). Based the sequencing data published by Flommersfeld et al. (GSE180978), a notable negative correlation was observed between the expression levels of Prdm1 and Batf3 (Figure 5—figure supplement 2I). On top of that, our findings unveiled the negative regulatory influence of Prdm1 on Batf3 within both spleen

and liver NK cells. This discovery highlights a potential upstream mechanism that may influence the hemostasis of the spleen NK cell subpopulations through Batf3.

We also compared the gene expression patterns between *Prdm1* and *Hobit* (homologue of Blimp1) with two published scRNA-seq data (50, 52). Following the knockout of Hobit, the DEGs were primarily identified within ILC1s. Conversely, after the knockout of Prdm1, a greater number of DEGs were observed in cNK cells. This indicates that Prdm1 likely possesses a broader range of target genes within cNK cells, whereas Hobit appears to have a more pronounced impact on gene expression within ILC1s (Figure 5—figure supplement 2, C-F). There are some overlaps between the downstream transcriptional profile of *Prdm1* and *Hobit* in liver cNK cells and ILC1s (Figure 5—figure supplement 2, G and H), such as *Junb*, *Fosb*, *Tcf7*, *Kit*, *Gzmb*, *Prf1*, and *Cxcr6* was simultaneously upregulated or downregulated in both *Prdm1*$^{\Delta Ncr1}$ and *Hobit*^{KO} liver cNK cells or ILC1s, indicating the similar regulatory networks of Prdm1 and Hobit.

Prdm1 **facilitates the intercellular communication between liver group 1 ILCs and macrophages**

The reciprocal crosstalk between group 1 ILCs and macrophages plays a critical role in maintaining liver immune homeostasis and anti-cancer immune surveillance (53, 54). The scRNA sequencing analysis identified two well-established subpopulations of liver macrophages: the resident Kupffer Cells (KCs) and the Monocyte-Derived Macrophages (MDMs) (Figure 6, A-C; Figure 6—figure supplement 1A). When comparing the total proportion of macrophages within the immune cell population of the liver between WT and *Prdm1*$^{\Delta Ncr1}$ mice, there is an increase in *Prdm1*$^{\Delta Ncr1}$ mice (Figure 6C). To confirm these findings, we utilized flow cytometry to define

macrophages, including both KCs and MDMs, gating by $CD45^{+}Ly6G^{-}F4/80^{+}CD11b^{+}$ (Figure 6D). Our analysis showed that, following the deletion of *Prdm1* in Group 1 ILCs, there is a significant increase in both the proportion and number of macrophages in the liver (Figure 6D).

According to the transcriptional profile, liver macrophages were further clustered and labeled as "*Ly6c2*^{hi}"; "*Cxcl2*^{hi}"; "*Ear2*^{hi}" MDMs, and "*Mrc1*^{hi}"; "*C1q*^{hi}" KCs (Figure 6A, Figure 6—figure supplement 1, A-E). Increased proportion of MDMs and KCs was observed in *Prdm1*$^{\Delta Ncr1}$ cells (Figure 6—figure supplement 1B). Within MDMs clusters, *Ly6c2*^{hi} MDMs mainly compose of *Prdm1*$^{+/+}$ cells, while *Prdm1*$^{\Delta Ncr1}$ cells concentrated in *Cxcl2*^{hi} cluster (Figure 6C). The scRNA-seq data reveal that following Prdm1 knockout in $NKp46^{+}$ cells, there is a decrease in the proportion of KCs within the macrophage population, while the proportion of MDMs increases (Figure 6D). CX3CR1, a chemokine receptor, is extensively utilized to distinguish KCs and MDMs within macrophages. Cells expressing CX3CR1 are identified as MDMs, whereas those without CX3CR1 expression are categorized as KCs (55). Employing flow cytometry and leveraging CX3CR1 expression, we assessed the ratios of KCs and MDMs. However, diverging from the scRNA-seq findings, flow cytometry indicates that post-Prdm1 knockout in group 1 ILCs, there is a minor increase in the proportion of KCs within the total liver macrophages, and a decrease in the proportion of MDMs (Figure 6D; Figure 6—figure supplement 1B). This discrepancy could stem from the different bases of classification: scRNA-seq defines KCs based on gene expression profiles, whereas flow cytometry differentiates between KCs and MDMs using the single surface marker, CX3CR1. Analysis of the macrophage subsets identified by scRNA-seq reveals that, while MDM clusters generally show high CX3CR1 expression, there exists a subset within MDMs, labeled *Mrc1*^{hi}, that also exhibits high levels of CX3CR1 (Figure 6—figure

supplement 1C). Consequently, if flow cytometry solely employs CX3CR1 for differentiating between KCs and MDMs, it could result in disparities when compared to scRNA-seq outcomes. Both KCs and MDMs has significantly increased in *Prdm1*$^{\Delta Ncr1}$ mice, which was consist with the scRNA-seq data (Figure 6—figure supplement 1, B and F). Despite the decrease in the proportion of *Ly6c2*^{hi} MDMs in *Prdm1*$^{\Delta Ncr1}$ mice, the expression levels of *Ly6c2* exhibited minimal variation between WT and *Prdm1*$^{\Delta Ncr1}$ mice (Figure 6—figure supplement 1D). Intriguingly, within certain cellular subsets, notably the *Ear2*^{hi} cluster, the *Ly6c2* expression levels in KO mice were found to be higher than those in WT mice. Additionally, we employed flow cytometry to examine Ly6C expression within the macrophages. Similar with the scRNA-seq findings, there were no notable differences in Ly6C expression levels between WT and KO mice (Figure 6E; Figure 6—figure supplement 1G).

High-resolution interactions among liver cNK cells, ILC1s, and macrophages were established and compared between *Prdm1*$^{+/+}$ and *Prdm1*$^{\Delta Ncr1}$ mice using the CellChat program (56). Interactions between ILC1s and total macrophages were higher than that between cNK cells and macrophages (Figure 6—figure supplement 2, A, C, E, and G). Cross-talk between liver group 1 ILCs with macrophages enriched in macrophage migration inhibitory factor (MIF), MHC-I, CXC chemokine ligand (CXCL), Thy-1 cell surface antigen (THY1), and C-type lectin (CLEC) pathways (Figure 6—figure supplement 2, B, D, F, and H). Although the quantity of macrophages significantly increases in *Prdm1*$^{\Delta Ncr1}$ mice, there is a significant decrease in the interaction number and interaction strength between liver group 1 ILCs and macrophages (~1.5 fold) in *Prdm1*$^{\Delta Ncr1}$ mice (Figure 6, F and G). The reduction of interaction mostly occurred in the cross-talk of ILC1-MDM and ILC1-KC, whereas no difference was observed in cNK-MDM and cNK-KC

interaction (Figure 6—figure supplement 2, A-H). A reduction in the interaction of ligand-receptor, such as Mif-CD74, Cxcl16-Cxcr6, and Cxcl10-Cxcr3 was observed in *Prdm1*$^{\Delta Ncr1}$ mice compared to *Prdm1*$^{+/+}$ mice (Figure 6—figure supplement 3). Compared to *Prdm1*$^{+/+}$ mice, the information flow of CXCL and MIF pathways significantly decreased in *Prdm1*$^{\Delta Ncr1}$ mice (Figure 6, H and I; Figure 6—figure supplement 2, B, D, F, and H). These pathways play a crucial role in facilitating macrophage migration. The CXCL signaling was sent from *Ly6c2*^{hi} *Cxcl2*^{hi} MDMs and *C1q*^{hi} KC, targeting all ILC1 clusters and *Cxcr3*^{hi} cNK cell clusters (Figure 6J). Of note, although the population of *Cxcl2*^{hi} macrophage primarily comprised cells from *Prdm1*$^{\Delta Ncr1}$ mice, the interaction within the CXCL pathway between macrophages and group 1 ILCs was obviously less than *Prdm1*$^{+/+}$ sample (Figure 6J). These changes could be linked to a decreased population of ILC1s and *Cxcr3*^{hi} cNK cell cluster in *Prdm1*$^{\Delta Ncr1}$ mice, implying that the homeostasis of *Cxcl2*^{hi} macrophages required sufficient signals from cNK cells and ILC1s. The impaired CXCL-CXCR interactions might subsequently lead to reduced recruitment and activation of group 1 ILCs and macrophages within the tumor microenvironment.

Prdm1 **safeguards group 1 ILCs from exhaustion-like phenotypes in the tumor microenvironment**

The suppression of mitochondrial related pathways in *Junb*^{hi} cNK cell cluster, along with a significant increase of this cNK cell cluster in *Prdm1*$^{\Delta Ncr1}$ mice, encouraged us to explore mitochondrial function through flow cytometry. MitoTracker, MitoSOX, and Tetramethylrhodamine methyl ester (TMRM) were used to assess the mitochondrial mass, superoxide production, and mitochondrial membrane potential. A substantial decrease in MFIs of

MitoTracker was observed in *Prdm1*$^{\Delta Ncr1}$ splenic cNK cells, liver cNK cells, and liver ILC1s when compared to their *Prdm1*$^{+/+}$ counterparts (Figure 7A). This observation aligns with the enrichment of downregulated genes from *Prdm1* deficient sample in mitochondrial related pathway, as revealed by RNA sequencing data (Figure 4—figure supplement 2, D-F). There was no significant difference in MitoSOX and TMRM between *Prdm1*$^{\Delta Ncr1}$ and *Prdm1*$^{+/+}$ mice (Figure 7, B and C), which suggested that the ATP synthesize capacity was minimally affected by *Prdm1*.

IFN-γ is a critical cytokine for NK cells mediated cancer surveillance(57, 58) and impaired production of IFN-γ was considered as a key hallmark of exhausted NK cells (59, 60). To evaluate the IFN-γ secreting capacity of liver cNK cells and ILC1s in tumor microenvironment, B16F10 tumor cells were inoculated to the liver via splenic injection and the IFN-γ levels in response to stimulation of IL-12 and/or IL-18 were assessed by flow cytometry (Figure 7—figure supplement 1A). The proportion changes of cNK cells and ILC1s in *Prdm1*$^{\Delta Ncr1}$ mice was similar with the no tumor-burden condition, while the number of both cNK cells and ILC1s have significant decreased in tumor-bearing liver (Figure 7D). Compared with *Prdm1*$^{+/+}$ mice, significant deceased of IFN-γ were observed in *Prdm1*$^{\Delta Ncr1}$ mice liver cNK cells and ILC1s under the combinate stimulation of IL-12/IL-18 (Figure 7E; Figure 7—figure supplement 1B), which was more remarkable in liver ILC1s. Similar trends were observed when IL-12 or IL-18 was used alone, although only liver ILC1s showed a significant decrease in response to IL-18 stimulation (Figure 7E). These findings were consistent with the heavy tumor burden observed in *Prdm1*$^{\Delta Ncr1}$ mice.

Discussion

Prdm1 is a pivotal transcription factor that has attracted substantial research interest due to its

role in lymphocytes. In a study involving systemic knockout combined with competitive transplantation, it was found that Prdm1 promotes NK cell maturation and the expression of Gzmb. On the contrary, the same study also found that NK cells with Prdm1 deficiency exhibit heightened proliferation, increased survival, enhanced migratory abilities towards tumors, and greater cytotoxicity against subcutaneously implanted RMAS tumors (30). Using Ncr1-driven conditional knockout transgenic mice, which specifically delete *Prdm1* in group 1 ILCs, we not only validated *Prdm1*'s positive regulation of NK cell maturation, but also demonstrated its indispensable role in NK cell anti-tumor activity. The compromised mitochondrial function and reduced IFN-γ, granzyme B, and perforin production appear to be potential contributing factors to Prdm1-mediated cancer surveillance. Reduction of CX3CR1^{+} NK cells in multiple tissues, and decreased expression of *Cx3cr1* and *Cxcr6* was observed in *Prdm1*$^{\Delta Ncr1}$ splenic cNK cells (Figure 3F), both of which are essential for NK cells egressing from bone marrow (61, 62). Our results not only confirmed a decrease in cytotoxic molecules in *Prdm1*-deficient NK cells (30) but also showed that the reduction in Gzmb and perforin is not solely attributable to the diminished maturation of these cells. Mature NK cells in bone marrow obtained the expression of CX3CR1 and acquired ability to enter the circulation (61, 62). The quantity of cNK cells increased exclusively in the bone marrow, with reductions observed in all other tissues (Figure 1G), indicating *Prdm1* might regulate chemokine receptors to facilitate the egression of cNK cells from the bone marrow to peripheral tissues. In addition, higher expression of *Cxcr6* compared to cNK cells is also a key factor for liver tissue residence of ILC1s (63). Decreased expression of *Cxcr6* in *Prdm1* deficient group 1 ILCs may also contribute to the balance shift towards cNK cells. Furthermore, although both liver NK cells and liver ILC1s require Prdm1 to maintain their

quantity, liver ILC1s demonstrate a more pronounced dependency on Prdm1. However, it is currently widely believed that liver NK cells and liver ILC1s originate from different progenitors. It is worth noting that while we observed changes in the NK and ILC1 proportions after *Prdm1* knockout, our data does not support the hypothesis that Prdm1 affects progenitor differentiation decisions, thereby influencing the fate selection of NK and ILC1. Further research may be needed to elucidate how Prdm1 regulates the balance between NK cells and ILC1s.

scRNA sequencing analysis reveals that both liver cNK cells and ILC1s can be further divided into three subgroups based on their gene expression patterns. Junb is a crucial transcriptional factor for the cytotoxic function of $CD8^+$ T cells and NK cells. However, excessive *Junb* expression has been found to promote T cell exhaustion (64). Our previous study showed that as NK cells mature, the expression level of *Prdm1* increased while the expression level of *Junb* gradually decreased (25). The current study demonstrated that in NK cells, the expression level of *Junb* significantly increases upon the deletion of Prdm1, indicating that *Junb* expression is suppressed by Prdm1. As *Junb* expression decreases with NK cell maturation, and it is inhibited by the gradually increasing Prdm1 during maturation. This implies that constraining *Junb* expression is likely a fundamental prerequisite for NK cell maturation. However, the precise mechanism by which Prdm1 downregulates *Junb* in NK cells still needs further research. Furthermore, $Junb^{hi}$ NK cells exhibit lower expression levels of cytotoxic genes and reduced mitochondrial-related signaling pathways. Mitochondria are pivotal organelles crucial for cellular metabolism. Disruptions in mitochondrial function have been linked to T Cell exhaustion, attributed to glycolytic reprogramming (65). Similarly, mitochondrial fragmentation has been closely associated with NK cell exhaustion (66). However, the concept of NK cell exhaustion isn't

as firmly established as it is for T cells. Exhausted NK cells should primarily exhibit diminished functions. This is characterized by a diminished ability to destroy tumor cells, a reduced capability to activate other components of the immune system, and compromised proliferation and survival rates. Additionally, this reduced functionality is associated with a decline in the expression of molecules responsible for cytotoxic activity, lower production of IFN-γ, and metabolic disturbances that may arise from mitochondrial dysfunction. While our current data is not sufficient to definitively classify these cells as exhausted NK cells, it supports that a subpopulation, referred to *Junb*^{hi} cluster, demonstrates an exhaustion-like phenotype. The significant increase in this cell population following *Prdm1* knockout in NK cells may potentially be one of the reasons why *Prdm1*$^{\Delta Ncr1}$ mice lose their tumor-killing capacity. Whether the excessive expression of JunB in NK cells is also a contributing factor to their exhaustion, similar to T cells(64), requires further investigation.

The scRNA-seq data revealed that *Prdm1* plays distinct roles in regulating cNK cells and ILC1s despite being required for the quantity of both lineages. Specifically, *Prdm1* appears to be more involved in promoting the resistance against exhaustion in cNK cells, whereas in ILC1s, it may play a role in the plasticity between ILC1s and ILC3s. In both our previous study and a study by Colonna et al. (25, 67), it was demonstrated that *Smad4*, a transcriptional factor involved in TGF-β signal pathway, upregulated *Prdm1* in NK cells and depletion of *Smad4* resulted in a decreased ratio of NK cells to ILC1s in the liver. However, knocking out *Prdm1* in Ncr1^{+} cells increased the ratio of NK cells to ILC1s in liver group 1 ILCs (Figure 2A). These findings suggest the possibility of a Smad4-independent pathway through which *Prdm1* promotes the maintenance of ILC1s, or that *Prdm1* plays a more significant role in maintaining ILC1s compared to its role in

NK cells.

Previous studies have identified Hobit and Prdm1 as central regulators instructing tissue-dependent programs and retention of diverse tissue-resident lymphocytes (17, 50, 52). Liver ILC1s required Hobit, but not necessary for cNK cells (6). Expression of Prdm1 was remarkably higher in cNK cells versus ILC1s (17). While in our study, cNK cells and liver ILC1s reduced simultaneously in *Prdm1*$^{\Delta Ncr1}$ mice, and even more significant in ILC1s. This indicates that while Prdm1 is expressed at lower levels in ILC1s, its role in preserving the quantity of ILC1s may be more crucial. Thus, Prdm1 and Hobit may have parallel program in instructing ILC1s functional development and maturation. Prdm1 and Hobit directly bound and repressed *Tcf7* (17), which encoded TCF-1, a TF binding and limiting the activity of Gzmb regulatory element (68). Gzmb has been demonstrated directly bound and activated by Junb in NK cells, which suggested Gzmb expression regulated by multiple Prdm1/Hobit downstream signals (25). In human T cells, binding motif of JUNB was enriched in the binding sites of PRDM1 (69), indicating the essential role of PRDM1-JUNB axis during NK cell and T cell development. In NK cells deficient in Prdm1 expression, we noted a decrease in Gzmb levels alongside with an elevation in Junb expression. This indicates that Prdm1 not only facilitates the expression of Gzmb in NK cells but also suppresses Junb expression. Given that Junb is recognized as a positive regulator of Gzmb (70), this presents a complex interplay that seems contradictory. Therefore, it is imperative to develop a theoretical framework to comprehensively understand and interpret this paradoxical relationship. Our previous research has demonstrated that with the progression of NK cell maturation, there is a gradual increase in Prdm1 expression, accompanied by a subtle reduction in JunB levels (25). Overexpression of Junb can induce lymphocyte exhaustion (64). Based on these findings, we

hypothesize that during the initial stages of NK cell development, JunB might enhance the expression of certain molecules associated with cytotoxicity, thereby aiding NK cells in acquiring the capacity to eliminate target cells. During these initial stages, Prdm1 level are comparatively low, thus exerting a weaker inhibitory effect on JunB. As NK cells proceed to maturity, there's a progressive increase in Prdm1 level, which then exerts a stronger inhibitory influence on JunB, contributing to the reduced JunB level in terminal matured NK cells. Consequently, this reduces the potential for NK cell exhaustion caused by elevated levels of JunB.

Chronic inflammation is a crucial factor in promoting tumorigenesis, and macrophages play a significant role in this process. Macrophages interact with both cNK cells and ILC1s. However, the TFs that regulate these interactions are poorly understood. Fortunately, recent advances in scRNA-seq technology and the CellChat software tool (56) have allowed us to gain a better understanding of the *Prdm1* signaling pathway in group 1 ILCs and its impact on macrophages at the transcriptional level. Increased metastasis in *Prdm1*$^{\Delta Ncr1}$ mice may be due to a decrease in the killing ability of NK cells, making them more prone to exhaustion, or it could be due to abnormalities in group 1 ILCs, leading to a decrease in the anti-tumor abilities of macrophages and an enhancement of their pro-tumor capabilities. It is worth noting that normal ILC1-macrophage interactions are more prevalent than the interaction between NK cells and macrophages (Figure 6—figure supplement 2). We also found that CXCL signaling based interaction remarkably diminished in *Prdm1*$^{\Delta Ncr1}$ mice, which suggested CXCL-CXCR may contribute to keep the sufficient interaction between group 1 ILC and macrophage. Specifically, *Prdm1* in group 1ILCs may be critical in preventing the overactivation of macrophages that can lead to cancer development. Increased population of both MDMs and KCs in *Prdm1*$^{\Delta Ncr1}$ mice, as

well as different distribution of macrophage clusters, indicating the homeostasis of macrophages require environment with functional cNK cells and ILC1s. Although not all macrophage phenotypes have been verified in this study, the present research serves primarily to offer initial insights and preliminary data for investigating the interactions between group 1 ILCs and macrophages. It aims to inspire further research into the role of transcription factors within the liver and the cancer microenvironment.

While our findings underscore the importance of Prdm1 in liver cNK cells and ILC1s tumor immune surveillance, it does not be validated in human NK cells, whereas previous studies have found that PRDM1 might inhibit the proliferation and function of human NK cells (32, 71). Furthermore, we not provided an in-depth evaluation in multiple tumor models. Further research may provide deeper insight into the role of PRDM1 in the anti-tumor function of human NK cells, enabling a more direct investigation of its application in cancer therapies. Given its important role in preserving liver cNK cells and ILC1s functional heterogeneity, enhancing Prdm1 function in human NK cells could potentially be a strategy to promote NK cell-based immunotherapy for cancer.

Methods

Mice

Prdm1$^{fl/fl}$ mice were purchased from The Jackson Laboratory. *Ncr1-iCre* and *B2m*$^{-/-}$ mice were purchased from Shanghai Model Organisms Center, Inc.. Six- to twelve-week-old littermates were used for the experiment.

Cell lines

B16F10 melanoma cells were obtained from ATCC (CRL-6475) and negative for mycoplasma contamination.

Experimental metastasis model

For lung metastasis model, 0.3×10^6 B16F10 cells were intravenous injected into mice. Three weeks later, mice were euthanized for analysis. For liver metastasis model, mice were inoculation with 0.5×10^6 B16F10 via intrasplenic injection. Three weeks later, mice were euthanized for analysis. Lung and liver from tumor-bearing mice were fixed in 10% formalin and embedded in paraffin. Sections were stained with H&E.

***In vivo* cytotoxicity assay**

Donor splenocytes harvested from B2m deficient (*B2m*$^{-/-}$) mice were labeled with 5 μM CFDA-SE. Donor splenocytes harvested from B2m-adequate (*B2m*$^{+/+}$) mice were labeled with 5 μM eF670. Labeled splenocytes from two mouse strains were mixed in a 1:1 ratio, and 1×10^7 cells in total were injected i.v. into *Prdm1*$^{+/+}$ and *Prdm1*$^{\Delta Ncr1}$ mice. One day after administration, spleen and liver cells were isolated from recipient mice, and the population of labeled cells was analyzed by flow cytometry. Rejection % was quantified according to the following formula:

$1\text{-}(\%B2m^{+/+}/\%B2m^{-/-})_{Prdm1^{+/+}\text{ or }Prdm1^{\Delta Ncr1}} \times 100\%$.

Cell isolation

Mice were perfused with 1◊ PBS by portal vein puncture before harvesting tissues. Liver and

lung was digested with 0.05% collagenase II for 30 minutes and filtered through 70 μm cell strainers, and mononuclear cells were isolated after subjected to density gradient using 30% and 70% percoll. Spleen were also removed and pressed through 70 μm filterers to obtain splenocytes. Peripheral blood mononuclear cells were obtained from peripheral blood after lysis of red blood cells (Biolegend, 420301). Flushing femurs and mechanical disruption of inguinal lymph nodes were performed to obtain cells from bone marrow and lymph nodes.

Real-time RT-PCR

RNA was extracted from FACS-sorted NK cells or splenocytes using RNASimple Total RNA Kit (TIANGEN Biotech, 4992858) and subsequently reverse transcribed to cDNA with SuperScript VILO Master Mix (Thermo Fisher Scientific, 11755050) according to manufacturer's instructions. qPCR was performed with SYBR Green Mix (Thermo Fisher Scientific, A25742) and CFX Opus 96 Real-Time PCR System (Bio-Rad). The relative mRNA expression level was calculated using 2^{-ddCt} method. Primer sequences: *Prdm1*: 5'-CAGAAACACTACTTGGTACA-3'; 5'-GATTGCTTGTGCTGCTAA-3'.

Flow cytometry

Flow cytometry and cell sorting were performed with a Cytoflex S/SRT (Beckman Coulter). The following antibodies were used (all purchased from BioLegend unless otherwise indicated): CD45-PE-Cy7 (catalog 103114, clone 30-F11); CD3ε-PerCP-Cy5.5 (catalog 100327, clone 145-2C11); NK1.1-BV421 (catalog 108741, clone PK136); CD335-AF647 (catalog 560755, clone 29A1.4, BD Bioscience); CD49a-PE (catalog 562115, clone Ha31/8, BD Bioscience);

CD49b-FITC (catalog 108906, clone DX5); CD27-BV510 (catalog 124229, clone LG.3A10); CD11b-AF700 (catalog 101222, clone M1/70); KLRG1-APC (catalog 561620, clone 2F1, BD Bioscience); CD49a-BV421 (catalog 740046, clone Ha31/8, BD Bioscience); IFN-γ-PE (catalog 505807, clone XMG1.2); Granzyme B (catalog 372207, clone QA16A02); Perforin (catalog 154305, clone S16009A); CD49b-APC-Cy7 (catalog 108919, clone DX5) ; IgG-PE (catalog 402203, clone 27-35); CD335-BV510 (catalog 137623, clone 29A1.4);; CD3ε-APC-Cy7 (catalog 100330, clone 145-2C11); CD11b-BV421 (catalog 101235, clone M1/70); CD3ε-BV421 (catalog 100335, clone 145-2C11); CD3ε-FITC (catalog 553061, clone 145-2C11, BD Bioscience); CX3CR1-PE (catalog 149005, clone SA011F11); Ly6G-PerCP-Cy5.5 (catalog 127615, clone 1A8); Ly6C-BV510 (catalog 108437, clone RB6-8C5); F4/80-APC-Cy7 (catalog 123118, clone BM8). For mitochondrial metabolic assay, fresh cells were incubated in 37□ media for 30min with 100 nM MitoTracker Green (catalog M7514, Invitrogen), 100 nM TMRM (catalog T668; Invitrogen), and 10 uM MitoSOX Red (catalog M36008; Invitrogen), respectively. Surface-stained after washing with PBS and then detected by flow cytometry. For intracellular IFN-γ staining, Cells freshly obtained from liver and spleen were stimulated 12 hours with or without cytokine. GolgiStop (BD Biosciences) was added 4 hours before intracellular staining.

Bulk RNA sequencing

Total RNA from FACS sorted splenic NK cells of *Prdm1*$^{+/+}$ and *Prdm1*$^{\Delta Ncr1}$ mice was extracted by TRIzol reagent (Invitrogen), then reverse transcribed into cDNA. Library construction was prepared using Illumina mRNA Library kit, and sequencing was performed by the BGISEQ-500. Standard methods were used to analyze the RNA-seq data, including aligning

the reads to the genome by HISAT2 (v2.1.0) (72), and gene expression values (Counts) were calculated using RSEM (v1.3.1) (73). DEGs were identified using DEseq2 (v1.4.5) (74) with a cutoff of $\log_2$(fold change) > 0.5 and P < 0.05. The "clusterProfiler" package (v4.4.4) (75) and gene sets from molecular signatures database (MSigDB) were used for GSEA and GO analysis. The heatmap was plotted using the "Pheatmap" package (v1.0.12).

Single-cell RNA sequencing

FACS-sorted liver $CD45^+$ cells with more than 80% cell viability were used for library preparation. Each sample contained cells from three *Prdm1*$^{+/+}$ or *Prdm1*$^{\Delta Ncr1}$ mice. Gel Bead-in-Emulsions (GEMs) were generated using the 10X Genomics Chromium system, which combinates Master Mix, Single Cell 3' v3.1 Gel Beads, and Partitioning Oil with single cells. GEMs were mixed with cell lysate and reverse transcription reagent to produce full-length cDNA. After incubation, the GEMs were broken, and recovered cDNA were amplified via PCR. Fragmentation, End repair, A-tailing, and Adaptor Ligation were performed to obtain final libraries, which contain P5 and P7 sequences. The 3' library was sequenced on Novaseq 6000 with approximately 50k read pairs/cell sequencing depth. The "Seurat" R package (v4.2.0) (76) was used for data analysis. Initial quality control was performed to filter out the low-quality cells and cell doublets. Cells with 200-5500 expressed genes and no more than 10% mitochondrial genes were considered for high-quality. Doublets were filtered with the "scDblFinder" Package (v1.10.0) (77). After quality control, we totally recovered 6161 cells and 4817 cells from *Prdm1*$^{+/+}$ and *Prdm1*$^{\Delta Ncr1}$ mice, respectively. Principal component analysis (PCA) was used for cluster analysis. The first 15 PCs were picked for clustering and further visualized by UMAP. Clusters-specific

marker was defined using the “FindAllMarkers” function, and clusters were manually annotated based on the top 30 or 15 markers. The “clusterProfiler” package and gene set from MSigDB were used for GSEA and GO analysis. “CellChat” package (v1.4.0) (56) was utilized to predict the cell-to-cell communication from scRNA-seq data.

TCGA datasets assay

The normalized gene expression and survival datasets of cancer patients collected in The Cancer Genome Atlas (TCGA) were downloaded from UCSC Xena (http://xena.ucsc.edu/) (78). NK cell-associated genes including *CD160*, *CD244*, *CTSW*, *FASLG*, *GZMA*, *GZMB*, *GZMH*, *IL18RAP*, *IL2RB*, *KIR2DL4*, *KLRB1*, *KLRC3*, *KLRD1*, *KLRF1*, *KLRK1*, *NCR1*, *NKG7*, *PRF1*, *XCL1*, *XCL2*, according to the previous study (33). NK cell-associated genes, together with *PRDM1*, constitute the *NK-PRDM1* signature in this study. The mean expression of per genes was ordered from high-to-low and plotted by heatmap using the “Pheatmap” package. The overall survival of patients in the high and low expression of *NK-PRDM1* signature was selected for analysis. Kaplan-Meier curves were plotted by GraphPad Prism.

Statistics

For experiment results, two-tailed t tests were used to measure the continuous and normally distributed between the two independent groups. Paired t-tests were used to determine the statistical significance between two paired groups. Log-rank tests were used to compare the overall survival distribution between the two groups of patients. A P value less than 0.05 was considered significant and data were presented as mean ± SEM.

Study approval

All animal experiments were approved by The Tianjin University Animal Care and Use Committee. No human subjects were performed in this study.

Data availability

Sequencing data have been deposited in Gene Expression Omnibus (GEO) dataset under accession codes GSE271233 (scRNA-seq) and GSE271380 (RNA-seq). All other data are available within the article and its supplementary information.

Author contributions

Jitian He, and Youwei Wang designed experiments, performed experiments, analyzed the data and wrote the manuscript. Jitian He, Le Gao, Peiying Wang, Yiran Zheng, Yumo Zhang, Xue Li, and Jiaman Sun performed experiments. Jitian He, Wing Keung Chan, Jiming Wang, Xiaohong Li, Huaiyong Chen, Zhouxin Yang, and Youwei Wang analyzed the data, interpreted results and reviewed the manuscript.

Acknowledgments

This work was supported by National Key Research and Development Plan of China (2022YFF1202901); National Natural Science Foundation of China (82372801); The Zhejiang Provincial Natural Science Foundation of China (LY21H150002); Natural Science Foundation of Tianjin (23JCYBJC01560, 23JCYBJC01370, 21JCZDJC00430); and Science and Technology Planning Project of Tianjin Municipal Education Commission (2022YGYB14)

Declaration of interests

The authors have declared that no conflict of interest exists.

References

1. Spits H, Artis D, Colonna M, Diefenbach A, Di Santo JP, Eberl G, et al. Innate lymphoid cells--a proposal for uniform nomenclature. *Nat Rev Immunol*. 2013;13(2):145-9.
2. Peng H, Jiang X, Chen Y, Sojka DK, Wei H, Gao X, et al. Liver-resident NK cells confer adaptive immunity in skin-contact inflammation. *J Clin Invest*. 2013;123(4):1444-56.
3. Bai L, Vienne M, Tang L, Kerdiles Y, Etiennot M, Escaliere B, et al. Liver type 1 innate lymphoid cells develop locally via an interferon-gamma-dependent loop. *Science*. 2021;371(6536).
4. Weizman OE, Adams NM, Schuster IS, Krishna C, Pritykin Y, Lau C, et al. ILC1 Confer Early Host Protection at Initial Sites of Viral Infection. *Cell*. 2017;171(4):795-808 e12.
5. Schuster IS, Wikstrom ME, Brizard G, Coudert JD, Estcourt MJ, Manzur M, et al. TRAIL+ NK cells control CD4+ T cell responses during chronic viral infection to limit autoimmunity. *Immunity*. 2014;41(4):646-56.
6. Ducimetiere L, Lucchiari G, Litscher G, Nater M, Heeb L, Nunez NG, et al. Conventional NK cells and tissue-resident ILC1s join forces to control liver metastasis. *Proc Natl Acad Sci U S A*. 2021;118(27).
7. Fumagalli V, Venzin V, Di Lucia P, Moalli F, Ficht X, Ambrosi G, et al. Group 1 ILCs regulate T cell-mediated liver immunopathology by controlling local IL-2 availability. *Science immunology*. 2022;7(68):eabi6112.
8. Kiessling R, Klein E, and Wigzell H. "Natural" killer cells in the mouse. I. Cytotoxic cells with specificity for mouse Moloney leukemia cells. Specificity and distribution according to genotype. *European journal of immunology*. 1975;5(2):112-7.
9. Nabekura T, Riggan L, Hildreth AD, O'Sullivan TE, and Shibuya A. Type 1 Innate Lymphoid Cells Protect Mice from Acute Liver Injury via Interferon-gamma Secretion for Upregulating Bcl-xL Expression in Hepatocytes. *Immunity*. 2020;52(1):96-108 e9.
10. Takeda K, Hayakawa Y, Smyth MJ, Kayagaki N, Yamaguchi N, Kakuta S, et al. Involvement of tumor necrosis factor-related apoptosis-inducing ligand in surveillance of tumor metastasis by liver natural killer cells. *Nat Med*. 2001;7(1):94-100.
11. Townsend MJ, Weinmann AS, Matsuda JL, Salomon R, Farnham PJ, Biron CA, et al. T-bet regulates the terminal maturation and homeostasis of NK and Valpha14i NKT cells. *Immunity*. 2004;20(4):477-94.
12. Yokota Y, Mansouri A, Mori S, Sugawara S, Adachi S, Nishikawa S, et al. Development of peripheral lymphoid organs and natural killer cells depends on the helix-loop-helix inhibitor Id2. *Nature*. 1999;397(6721):702-6.
13. Gascoyne DM, Long E, Veiga-Fernandes H, de Boer J, Williams O, Seddon B, et al. The basic leucine zipper transcription factor E4BP4 is essential for natural killer cell development. *Nature immunology*. 2009;10(10):1118-24.
14. Constantinides MG, McDonald BD, Verhoef PA, and Bendelac A. A committed precursor to innate lymphoid cells. *Nature*. 2014;508(7496):397-401.
15. Gordon SM, Chaix J, Rupp LJ, Wu J, Madera S, Sun JC, et al. The transcription factors T-bet and Eomes control key checkpoints of natural killer cell maturation. *Immunity*. 2012;36(1):55-67.

16. Daussy C, Faure F, Mayol K, Viel S, Gasteiger G, Charrier E, et al. T-bet and Eomes instruct the development of two distinct natural killer cell lineages in the liver and in the bone marrow. *J Exp Med*. 2014;211(3):563-77.
17. Mackay LK, Minnich M, Kragten NA, Liao Y, Nota B, Seillet C, et al. Hobit and Blimp1 instruct a universal transcriptional program of tissue residency in lymphocytes. *Science*. 2016;352(6284):459-63.
18. Lee JC, Green MD, Huppert LA, Chow C, Pierce RH, and Daud AI. The Liver-Immunity Nexus and Cancer Immunotherapy. *Clin Cancer Res*. 2022;28(1):5-12.
19. Galon J, and Bruni D. Approaches to treat immune hot, altered and cold tumours with combination immunotherapies. *Nature reviews Drug discovery*. 2019;18(3):197-218.
20. Ruff SM, Shannon AH, Beane JD, and Pawlik TM. Highlighting novel targets in immunotherapy for liver cancer. *Expert review of gastroenterology & hepatology*. 2022;16(11-12):1029-41.
21. He Y, Zhan L, Shi J, Xiao M, Zuo R, Wang C, et al. The Combination of R848 with Sorafenib Enhances Antitumor Effects by Reprogramming the Tumor Immune Microenvironment and Facilitating Vascular Normalization in Hepatocellular Carcinoma. *Adv Sci (Weinh)*. 2023:e2207650.
22. Nersesian S, Schwartz SL, Grantham SR, MacLean LK, Lee SN, Pugh-Toole M, et al. NK cell infiltration is associated with improved overall survival in solid cancers: A systematic review and meta-analysis. *Transl Oncol*. 2021;14(1):100930.
23. Lee HA, Goh HG, Lee YS, Jung YK, Kim JH, Yim HJ, et al. Natural killer cell activity is a risk factor for the recurrence risk after curative treatment of hepatocellular carcinoma. *BMC Gastroenterol*. 2021;21(1):258.
24. Gao Y, Souza-Fonseca-Guimaraes F, Bald T, Ng SS, Young A, Ngiow SF, et al. Tumor immunoevasion by the conversion of effector NK cells into type 1 innate lymphoid cells. *Nature immunology*. 2017;18(9):1004-15.
25. Wang Y, Chu J, Yi P, Dong W, Saultz J, Wang Y, et al. SMAD4 promotes TGF-beta-independent NK cell homeostasis and maturation and antitumor immunity. *J Clin Invest*. 2018;128(11):5123-36.
26. Cortez VS, Ulland TK, Cervantes-Barragan L, Bando JK, Robinette ML, Wang Q, et al. SMAD4 impedes the conversion of NK cells into ILC1-like cells by curtailing non-canonical TGF-beta signaling. *Nat Immunol*. 2017;18(9):995-1003.
27. Keller AD, and Maniatis T. Identification and characterization of a novel repressor of beta-interferon gene expression. *Genes Dev*. 1991;5(5):868-79.
28. Kallies A, Hawkins ED, Belz GT, Metcalf D, Hommel M, Corcoran LM, et al. Transcriptional repressor Blimp-1 is essential for T cell homeostasis and self-tolerance. *Nat Immunol*. 2006;7(5):466-74.
29. Martins GA, Cimmino L, Shapiro-Shelef M, Szabolcs M, Herron A, Magnusdottir E, et al. Transcriptional repressor Blimp-1 regulates T cell homeostasis and function. *Nat Immunol*. 2006;7(5):457-65.
30. Kallies A, Carotta S, Huntington ND, Bernard NJ, Tarlinton DM, Smyth MJ, et al. A role for Blimp1 in the transcriptional network controlling natural killer cell maturation. *Blood*. 2011;117(6):1869-79.
31. Akman B, Hu X, Liu X, Hatipoglu T, You H, Chan WC, et al. PRDM1 decreases sensitivity of

human NK cells to IL2-induced cell expansion by directly repressing CD25 (IL2RA). *Journal of leukocyte biology.* 2021;109(5):901-14.

32. Smith MA, Maurin M, Cho HI, Becknell B, Freud AG, Yu J, et al. PRDM1/Blimp-1 controls effector cytokine production in human NK cells. *J Immunol*. 2010;185(10):6058-67.

33. Cursons J, Souza-Fonseca-Guimaraes F, Foroutan M, Anderson A, Hollande F, Hediyeh-Zadeh S, et al. A Gene Signature Predicting Natural Killer Cell Infiltration and Improved Survival in Melanoma Patients. *Cancer Immunol Res.* 2019;7(7):1162-74.

34. Shapiro-Shelef M, Lin K-I, McHeyzer-Williams LJ, Liao J, McHeyzer-Williams MG, and Calame K. Blimp-1 Is Required for the Formation of Immunoglobulin Secreting Plasma Cells and Pre-Plasma Memory B Cells. *Immunity.* 2003;19(4):607-20.

35. Hayakawa Y, and Smyth MJ. CD27 dissects mature NK cells into two subsets with distinct responsiveness and migratory capacity. *J Immunol*. 2006;176(3):1517-24.

36. Chiossone L, Chaix J, Fuseri N, Roth C, Vivier E, and Walzer T. Maturation of mouse NK cells is a 4-stage developmental program. *Blood.* 2009;113(22):5488-96.

37. Huntington ND, Tabarias H, Fairfax K, Brady J, Hayakawa Y, Degli-Esposti MA, et al. NK cell maturation and peripheral homeostasis is associated with KLRG1 up-regulation. *J Immunol*. 2007;178(8):4764-70.

38. Bix M, Liao NS, Zijlstra M, Loring J, Jaenisch R, and Raulet D. Rejection of class I MHC-deficient haemopoietic cells by irradiated MHC-matched mice. *Nature*. 1991;349(6307):329-31.

39. Bern MD, Parikh BA, Yang L, Beckman DL, Poursine-Laurent J, and Yokoyama WM. Inducible down-regulation of MHC class I results in natural killer cell tolerance. *The Journal of experimental medicine.* 2019;216(1):99-116.

40. Karre K, Ljunggren HG, Piontek G, and Kiessling R. Selective rejection of H-2-deficient lymphoma variants suggests alternative immune defence strategy. *Nature*. 1986;319(6055):675-8.

41. Viant C, Fenis A, Chicanne G, Payrastre B, Ugolini S, and Vivier E. SHP-1-mediated inhibitory signals promote responsiveness and anti-tumour functions of natural killer cells. *Nat Commun*. 2014;5:5108.

42. Cillo C, Dick JE, Ling V, and Hill RP. Generation of drug-resistant variants in metastatic B16 mouse melanoma cell lines. *Cancer Res.* 1987;47(10):2604-8.

43. Sathe P, Delconte RB, Souza-Fonseca-Guimaraes F, Seillet C, Chopin M, Vandenberg CJ, et al. Innate immunodeficiency following genetic ablation of Mcl1 in natural killer cells. *Nat Commun*. 2014;5:4539.

44. Robinette ML, Fuchs A, Cortez VS, Lee JS, Wang Y, Durum SK, et al. Transcriptional programs define molecular characteristics of innate lymphoid cell classes and subsets. *Nat Immunol*. 2015;16(3):306-17.

45. Klose CS, Kiss EA, Schwierzeck V, Ebert K, Hoyler T, d'Hargues Y, et al. A T-bet gradient controls the fate and function of CCR6-RORgammat+ innate lymphoid cells. *Nature*. 2013;494(7436):261-5.

46. Chen Y, Wang X, Hao X, Li B, Tao W, Zhu S, et al. Ly49E separates liver ILC1s into embryo-derived and postnatal subsets with different functions. *The Journal of experimental medicine*. 2022;219(5).

47. Bottcher JP, Bonavita E, Chakravarty P, Blees H, Cabeza-Cabrerizo M, Sammicheli S, et al.

NK Cells Stimulate Recruitment of cDC1 into the Tumor Microenvironment Promoting Cancer Immune Control. *Cell*. 2018;172(5):1022-37 e14.

48. Kirchhammer N, Trefny MP, Natoli M, Brucher D, Smith SN, Werner F, et al. NK cells with tissue-resident traits shape response to immunotherapy by inducing adaptive antitumor immunity. *Sci Transl Med.* 2022;14(653):eabm9043.

49. Di Censo C, Marotel M, Mattiola I, Muller L, Scarno G, Pietropaolo G, et al. Granzyme A and CD160 expression delineates ILC1 with graded functions in the mouse liver. *European journal of immunology.* 2021;51(11):2568-75.

50. Friedrich C, Taggenbrock R, Doucet-Ladeveze R, Golda G, Moenius R, Arampatzi P, et al. Effector differentiation downstream of lineage commitment in ILC1s is driven by Hobit across tissues. *Nat Immunol.* 2021;22(10):1256-67.

51. Flommersfeld S, Bottcher JP, Ersching J, Flossdorf M, Meiser P, Pachmayr LO, et al. Fate mapping of single NK cells identifies a type 1 innate lymphoid-like lineage that bridges innate and adaptive recognition of viral infection. *Immunity.* 2021;54(10):2288-304 e7.

52. Yomogida K, Bigley TM, Trsan T, Gilfillan S, Cella M, Yokoyama WM, et al. Hobit confers tissue-dependent programs to type 1 innate lymphoid cells. *Proc Natl Acad Sci U S A.* 2021;118(50).

53. Tu Z, Bozorgzadeh A, Pierce RH, Kurtis J, Crispe IN, and Orloff MS. TLR-dependent cross talk between human Kupffer cells and NK cells. *J Exp Med*. 2008;205(1):233-44.

54. Park MD, Reyes-Torres I, LeBerichel J, Hamon P, LaMarche NM, Hegde S, et al. TREM2 macrophages drive NK cell paucity and dysfunction in lung cancer. *Nat Immunol*. 2023;24(5):792-801.

55. Heymann F, Peusquens J, Ludwig-Portugall I, Kohlhepp M, Ergen C, Niemietz P, et al. Liver inflammation abrogates immunological tolerance induced by Kupffer cells. *Hepatology.* 2015;62(1):279-91.

56. Jin S, Guerrero-Juarez CF, Zhang L, Chang I, Ramos R, Kuan CH, et al. Inference and analysis of cell-cell communication using CellChat. *Nat Commun*. 2021;12(1):1088.

57. Takeda K, Nakayama M, Sakaki M, Hayakawa Y, Imawari M, Ogasawara K, et al. IFN-gamma production by lung NK cells is critical for the natural resistance to pulmonary metastasis of B16 melanoma in mice. *Journal of leukocyte biology.* 2011;90(4):777-85.

58. Lin Q, Rong L, Jia X, Li R, Yu B, Hu J, et al. IFN-gamma-dependent NK cell activation is essential to metastasis suppression by engineered Salmonella. *Nature communications.* 2021;12(1):2537.

59. Roe K. NK-cell exhaustion, B-cell exhaustion and T-cell exhaustion-the differences and similarities. *Immunology.* 2022;166(2):155-68.

60. Zhang Q, Bi J, Zheng X, Chen Y, Wang H, Wu W, et al. Blockade of the checkpoint receptor TIGIT prevents NK cell exhaustion and elicits potent anti-tumor immunity. *Nature Immunology.* 2018;19(7):723-32.

61. Sciume G, De Angelis G, Benigni G, Ponzetta A, Morrone S, Santoni A, et al. CX3CR1 expression defines 2 KLRG1+ mouse NK-cell subsets with distinct functional properties and positioning in the bone marrow. *Blood*. 2011;117(17):4467-75.

62. Chea S, Possot C, Perchet T, Petit M, Cumano A, and Golub R. CXCR6 Expression Is Important for Retention and Circulation of ILC Precursors. *Mediators Inflamm.* 2015;2015:368427.

63. Hudspeth K, Donadon M, Cimino M, Pontarini E, Tentorio P, Preti M, et al. Human liver-resident CD56(bright)/CD16(neg) NK cells are retained within hepatic sinusoids via the engagement of CCR5 and CXCR6 pathways. *Journal of autoimmunity.* 2016;66:40-50.
64. Lynn RC, Weber EW, Sotillo E, Gennert D, Xu P, Good Z, et al. c-Jun overexpression in CAR T cells induces exhaustion resistance. *Nature.* 2019;576(7786):293-300.
65. Wu H, Zhao X, Hochrein SM, Eckstein M, Gubert GF, Knopper K, et al. Mitochondrial dysfunction promotes the transition of precursor to terminally exhausted T cells through HIF-1alpha-mediated glycolytic reprogramming. *Nature communications.* 2023;14(1):6858.
66. Zheng X, Qian Y, Fu B, Jiao D, Jiang Y, Chen P, et al. Mitochondrial fragmentation limits NK cell-based tumor immunosurveillance. *Nature immunology.* 2019;20(12):1656-67.
67. Cheng HP, Huang CJ, Tsai ML, Ong HT, Cheong SK, Choo KB, et al. MicroRNA-362 negatively and positively regulates SMAD4 expression in TGF-beta/SMAD signaling to suppress cell migration and invasion. *Int J Med Sci.* 2021;18(8):1798-809.
68. Jeevan-Raj B, Gehrig J, Charmoy M, Chennupati V, Grandclement C, Angelino P, et al. The Transcription Factor Tcf1 Contributes to Normal NK Cell Development and Function by Limiting the Expression of Granzymes. *Cell reports.* 2017;20(3):613-26.
69. Guo H, Wang M, Wang B, Guo L, Cheng Y, Wang Z, et al. PRDM1 Drives Human Primary T Cell Hyporesponsiveness by Altering the T Cell Transcriptome and Epigenome. *Front Immunol.* 2022;13:879501.
70. Babichuk CK, and Bleackley RC. Mutational analysis of the murine granzyme B gene promoter in primary T cells and a T cell clone. *J Biol Chem.* 1997;272(30):18564-71.
71. Kucuk C, Iqbal J, Hu X, Gaulard P, De Leval L, Srivastava G, et al. PRDM1 is a tumor suppressor gene in natural killer cell malignancies. *Proc Natl Acad Sci U S A.* 2011;108(50):20119-24.
72. Kim D, Langmead B, and Salzberg SL. HISAT: a fast spliced aligner with low memory requirements. *Nat Methods.* 2015;12(4):357-60.
73. Li B, and Dewey CN. RSEM: accurate transcript quantification from RNA-Seq data with or without a reference genome. *BMC Bioinformatics.* 2011;12:323.
74. Love MI, Huber W, and Anders S. Moderated estimation of fold change and dispersion for RNA-seq data with DESeq2. *Genome Biol.* 2014;15(12):550.
75. Wu T, Hu E, Xu S, Chen M, Guo P, Dai Z, et al. clusterProfiler 4.0: A universal enrichment tool for interpreting omics data. *Innovation (Camb).* 2021;2(3):100141.
76. Hao Y, Hao S, Andersen-Nissen E, Mauck WM, 3rd, Zheng S, Butler A, et al. Integrated analysis of multimodal single-cell data. *Cell.* 2021;184(13):3573-87 e29.
77. Germain PL, Lun A, Garcia Meixide C, Macnair W, and Robinson MD. Doublet identification in single-cell sequencing data using scDblFinder. *F1000Res.* 2021;10:979.
78. Caicedo HH, Hashimoto DA, Caicedo JC, Pentland A, and Pisano GP. Overcoming barriers to early disease intervention. *Nat Biotechnol.* 2020;38(6):669-73.

Figure legends

Figure 1. *Prdm1* promotes NK cell homeostasis and terminal maturation.

(**A**) Correlation between the average expression of NK cell-associated signature and *PRDM1* in LIHC (Liver Hepatocellular Carcinoma; n=363) patients sourced from TCGA datasets. (**B**) Heatmap of the ordered, z-score normalized expression values for *PRDM1* and NK cell-associated genes in liver cancer patients. High and low expression of *NK-PRDM1* signature are indicated. (**C**) Prognostic value of the *NK-PRDM1* signature for overall survival of liver cancer patients comparing high and low samples with a median cutoff. (**D**) Schematic representation of the Prdm1-conditional knockout mouse model. Targeted exon 6-8 of *Prdm1* (top) is flanked with *loxP* sites (middle). Ncr1-expressed Cre recombinase was used to generate the $Prdm1^{\Delta Ncr1}$ allele (bottom). (**E** and **F**) Real-time RT-PCR quantification of *Prdm1* expression in $NKp46^{+}$ cells (**E**) and splenocytes (**F**) to determine the presence of *Prdm1* (n=5). (**G**) Representative flow cytometric plots (left) and quantification (right) of the proportion and absolute number of $CD45^{+}CD3^{-}NKp46^{+}$ cells among lymphocytes in liver, lung, and bone marrow (n=10). (**H**) Representative flow cytometric plots (left) of the CD11b and CD27 expression within $CD3^{-}NK1.1^{+}NKp46^{+}CD49b^{+}$ cells in liver, lung, and bone marrow (n=10). Right panel showed the percentage of distinct maturation stages of NK cells. Data are presented as the mean±SEM and were analyzed by 2-tailed, paired t-test. Differences were evaluated between littermates. Each circle and square on graphs represents an individual mouse; *P*, *P*-value; r, pearson correlation coefficient; *, $P<0.05$; **, $P<0.01$, ns, not significant.

Figure 2. *Prdm1* is required for group 1 ILCs to control tumor metastasis.

(**A**) Representative flow cytometric plots (left) of liver cNK cells ($CD49a^{-}CD49b^{+}$) and ILC1s ($CD49a^{+}CD49b^{-}$) from $Prdm1^{+/+}$ and $Prdm1^{\Delta Ncr1}$ mice. The two bar graphs (right) quantitate the percentages and absolute numbers of cells respectively (n=7). (**B** and **D**) Representative image (left) and quantification (right) of tumor nodes on the livers (n=7) (**B**) and lungs (n=10) (**D**) of $Prdm1^{+/+}$ and $Prdm1^{\Delta Ncr1}$ mice at day 14 or 21 after inoculation with B16F10 melanoma cells. (**C** and **E**) Representative histopathological images of liver (**C**) and lung (**E**) tissues stained by hematoxylin-eosin to detect tumor metastasis. Red bar indicates 500 μm distance under the microscope. (**F**) Liver cells and splenocytes were co-stimulated in the presence or absence of IL-12 and IL-18 for 12 hours. GolgiStop was added 4 hours before intracellular staining of IFN-γ. The graphs showed percentage of $IFN\text{-}\gamma^{+}$ splenic cNK cells, liver cNK cells and ILC1s from $Prdm1^{+/+}$ and $Prdm1^{\Delta Ncr1}$ mice (n=5). Data are presented as the mean±SEM and were analyzed by 2-tailed, paired t-test. Differences were evaluated between littermates. Each circle and square on graphs represents an individual mouse; *P*, *P*-value; *, $P<0.05$; **, $P<0.01$, ns, not significant.

Figure 3. Bulk RNA-seq reveals Prdm1-mediated functions in splenic cNK cells.

(**A**) Splenic cNK cells and liver CD45$^+$ cells were sorted from *Prdm1*$^{+/+}$ and *Prdm1*$^{\Delta Ncr1}$ mice using flow cytometry, and prepared for bulk RNA-seq and single-cell RNA-seq analysis. (**B**) Volcano plot of the bulk RNA-seq differentially expressed genes (DEGs) ($\log_2$|fold change|>0.5; P<0.05) in splenic cNK cells between *Prdm1*$^{+/+}$ and *Prdm1*$^{\Delta Ncr1}$ mice. Upregulated and downregulated genes in *Prdm1*$^{\Delta Ncr1}$ cells were highlighted in red and blue. (**C**) Enriched Gene Ontology (GO) terms of DEGs in *Prdm1*$^{\Delta Ncr1}$ cells compared *Prdm1*$^{+/+}$ cells. The Enrichment gene set in upregulated (red) and downregulated (blue) genes were indicated in different colour. Bar length represents statistical significance. (**D**) Gene Set Enrichment Analysis (GSEA) showing the enrichment of NF-kappa B signaling pathway of DEGs in *Prdm1*$^{\Delta Ncr1}$ cells compared *Prdm1*$^{+/+}$ cells. NES, normalized enrichment score. (**E**) Heatmap of selected genes from DEGs. Shown is z-score transformed expression of DEGs. (**F**) Representative flow cytometric plots (left) and cumulative data (right) of the percentage and absolute numbers of CX3CR1$^+$ cells in liver cNK cells and ILC1s (n=5). (**G**) Quantification of CX3CR1$^+$ cells in NK cells in blood, bone marrow, lung, liver, spleen, and lymph nodes (n=5). (**H** and **I**) Representative flow cytometric plots (left) and cumulative data (right) showing the proportion of GZMB$^+$ (**H**) and PRF1$^+$ (**J**) liver cNK cells and ILC1s from *Prdm1*$^{+/+}$ and *Prdm1*$^{\Delta Ncr1}$ mice (n=5). (**J** and **K**) Proportion of GZMB$^+$ (**J**) and PRF1$^+$ (**K**) splenic NK cells at different maturation stages was analyzed by flow cytometry (n=5). Data are presented as the mean±SEM and were analyzed by 2-tailed, paired t-test. Differences were evaluated between littermates. Each circle and square on graphs represents an individual mouse; P, P-value; *, P<0.05; **, P<0.01, ns, not significant.

Figure 4. Different properties of cNK clusters following *Prdm1* knockout.

(**A**) Uniform manifold approximation and projection (UMAP) visualization of liver CD45$^+$ cells from *Prdm1*$^{+/+}$ and *Prdm1*$^{\Delta Ncr1}$ mice. Twelve clusters were defined and indicated by distinct colours. Each dot represents a single cell. (**B**) UMAP visualization of liver cNK and ILC1 clusters. Cells were colored by genotypes (*Prdm1*$^{+/+}$-blue; *Prdm1*$^{\Delta Ncr1}$-red). (**C**) Percentages of cNK cells and ILC1s in total group 1 ILCs (left), and their distribution in each cluster (right). (**D** and **E**) UMAP visualization of three different liver cNK clusters from two mouse strains. (**F**) Proportions of cNK cells among total cNK cells (left; 211 cells in *Prdm1*$^{+/+}$, and 141 cells in *Prdm1*$^{\Delta Ncr1}$) and within clusters (right). (**G**) Violin plots showing the normalized expression of select genes in different cNK clusters. (**H**) Enriched GO term of marker genes in three cNK clusters. Dot size represents enriched gene number, and color intensity represents significance. (**I-L**) GSEA plots (left) depicting the enrichment of NF-kappa B (**I**) , TNF (**J**) , IL-17 (**K**) , and MAPK (**L**) signaling pathway in *Junb*^{hi} cNK cluster compared with clusters of *Prf1*^{hi} and *Cxcr3*^{hi} cNK cells. Right panel showed dynamic relative expression of the given gene sets from cluster1 to cluster3 between *Prdm1*$^{+/+}$ and *Prdm1*$^{\Delta Ncr1}$. Dots represent the average expression of given gene set in each cell, which was calculated through the sum of normalized expression of each individual gene within the designated gene set in every single cell. NES, normalized enrichment score.

Figure 5. Different properties of ILC1 clusters following *Prdm1* knockout.

(**A and B**) UMAP visualization of three different liver ILC1 clusters from two mouse strains. (**C**) Proportions of ILC1s among total ILC1s in different genotypes (left; 114 cells in *Prdm1*$^{+/+}$, and 63 cells in *Prdm1*$^{\Delta Ncr1}$) and within each cluster (right). (**D**) Violin plots showing the normalized expression of select genes in different ILC1 clusters. (**E**) Ridge plots showing the normalized expression of *Gzmb*, *Prf1*, and *Junb* in cNK and ILC1 clusters between *Prdm1*$^{+/+}$ and *Prdm1*$^{\Delta Ncr1}$ cells. (**F** and **G**) GSEA plots (left) depicting the enrichment of IL-17 signaling pathway (**F**) and T cell differentiation (**G**) in *Il7r*^{hi} ILC1 cluster compared with clusters of *Klra*^{hi} and *Gzmb*^{hi} ILC1s. Right panel showed dynamic relative expression of the given gene sets from cluster1 to cluster3 between *Prdm1*$^{+/+}$ and *Prdm1*$^{\Delta Ncr1}$. Dots represent the average expression of given gene set in each cell, which was calculated through the sum of normalized expression of each individual gene within the designated gene set in every single cell. NES, normalized enrichment score. (**H**) Enriched GO term of marker genes in three ILC1 clusters. Dot size represents enriched gene number, and color intensity represents significance. (**I**) Violin plot showing the *Junb*^{hi} signature score for cNK cell and ILC1 clusters, calculated using the signature genes of *Junb*^{hi} cNK cluster. (**J**) Venn diagram showing overlapping and unique DEGs in comparisons within liver cNK cells, ILC1s and splenic cNK cells between *Prdm1*$^{+/+}$ and *Prdm1*$^{\Delta Ncr1}$(left), and 17 overlapped DEGs were shown at the right panel.

Figure 6. *Prdm1* facilitates the intercellular communication between liver group 1 ILCs and macrophages.

(**A** and **B**) UMAP visualization of monocyte-derived macrophages (MDMs) and Kupffer cells (KCs) cluster (**A**) between *Prdm1*$^{+/+}$ and *Prdm1*$^{\Delta Ncr1}$ (**B**). (**C**) Proportions of total macrophages in liver immune cells (left), and proportions of MDMs and KCs among total macrophages in different genotypes (510 cells in *Prdm1*$^{+/+}$, and 624 cells in *Prdm1*$^{\Delta Ncr1}$). (**D**) Representative flow cytometric plots (left) and cumulative data (right) of the percentage and absolute numbers of liver total macrophages (CD45^{+}Ly6G^{-}CD11b^{+}F4/80^{+}), MDMs (CX3CR1^{-}), and KCs (CX3CR1^{+}) between *Prdm1*$^{+/+}$ and *Prdm1*$^{\Delta Ncr1}$ (n=7). (**E**) Representative flow cytometric plots (left) and cumulative data (right) of the percentage and absolute numbers of Ly6C^{-} and Ly6C^{+} cells in MDMs. (**F** and **G**) Circle plots (**F**) and summary data (**G**) illustrating the interaction numbers and strength of significant enriched ligand–receptor pairs among cluster of liver cNK cells, ILC1s, and macrophages from *Prdm1*$^{+/+}$ (left) and *Prdm1*$^{\Delta Ncr1}$ (right) cells. The thickness of the line indicates the number of enrich pairs, and the arrow reflects the direction of the interaction. (**H**) Heatmap of overall signaling pattern recognized from ligand-receptor pairs, which contained the sum of signaling from the sender and target cells. (**I**) Bar graphs showing the information flow in selected active signaling patterns between *Prdm1*$^{+/+}$ and *Prdm1*$^{\Delta Ncr1}$ cells. Relative information flow was calculated as the sum of the communication probability in given signaling patterns. (**J**) Chord plot of the CXCL signaling interaction network among cluster of liver cNK cells, ILC1s, and macrophages between *Prdm1*$^{+/+}$ and *Prdm1*$^{\Delta Ncr1}$ cells. Data are presented as the mean±SEM and were analyzed by 2-tailed, paired t-test. Differences were evaluated between littermates. Each

circle and square on graphs represents an individual mouse; *P*, *P*-value; *, *P*<0.05; **, *P*<0.01, ns, not significant.

Figure 7. *Prdm1* safeguards group 1 ILCs from exhaustion-like phenotypes in the tumor microenvironment.

(A-C) The Mitochondrial mass (MitoTracker Green staining; n=8) (**A**), Mitochondrial ROS (MitoSOX staining; n=5) (**B**), and Mitochondrial membrane potential (TMRM staining; n=5) (**C**) of splenic cNK cells, liver cNK cells and ILC1s were analyzed by flow cytometry. Representative flow cytometric plots (left) and cumulative data (right) showing the relative mean fluorescence intensities (MFIs) of each group. (**D**) Representative flow cytometric plots (left) and cumulative data (right) showing the percentage and absolute number of liver cNK cells and ILC1s in *Prdm1*$^{+/+}$ and *Prdm1*$^{\Delta Ncr1}$ tumor-bearing mice at day 14 after inoculation with B16F10 melanoma cells via intrasplenic injection(n=5). (**E**) Percentages of IFN-γ^{+} liver cNK cells and ILC1s from *Prdm1*$^{+/+}$ and *Prdm1*$^{\Delta Ncr1}$ tumor-bearing mice (n=5). Data are presented as the mean±SEM and were analyzed by 2-tailed, paired t-test. Differences were evaluated between littermates. Each circle and square on graphs represents an individual mouse; *P*, *P*-value; *, *P*<0.05; **, *P*<0.01, ns, not significant.

Figure 1—figure supplement 1. High expression of *PRDM1-NK* signature predicts better overall survival of cancer patients.

(**A and D**) Correlation between the average expression of NK cell-associated signature and *PRDM1* in lung adenocarcinoma (**A**) (LUAD, n=497) and skin cutaneous melanoma (SKCM, n=454) (**D**) patients from TCGA datasets. (**B and E**) Heatmap of the ordered, z-score normalized expression values for *PRDM1* and NK cell-associated genes in LUAD (**B**) and SKCM (**E**) patients. High and low expression of *NK-PRDM1* signature are indicated. (**C and F**) Prognostic value of the *NK-PRDM1* signature for overall survival of LUAD (**C**) and SKCM (**F**) patients comparing high and low samples with a median cutoff. (**G-I**) Prognostic value of the *NK-PRDM1* signature for overall survival of LIHC (**G**), LUAD (**H**), and SKCM (**I**) patients comparing high and low samples with a quartile cutoff. *P*, *P*-value; r, pearson correlation coefficient.

Figure 1—figure supplement 2. *Prdm1* plays an essential role in group 1 ILCs homeostasis and maturation.

(**A**) Representative flow cytometric plots (left) and quantification (right) of the proportion and absolute number of CD45^{+}CD3^{-}NKp46^{+} cells among lymphocytes in liver, lung, and bone marrow (n=10). (**B**) Representative flow cytometric plots (left) of the CD11b and CD27 expression within CD3^{-}NK1.1^{+}NKp46^{+}CD49b^{+} cells in liver, lung, and bone marrow (n=10). Right panel showed the percentage of distinct maturation stages of NK cells. **(C)** Representative flow cytometry

analyses of KLRG1^{+} cells in CD3^{-}NK1.1^{+}NKp46^{+}CD49b^{+} cells in liver, and their quantification in blood, bone marrow, lung, liver, spleen, and lymph nodes (n=5). (**D-G**) Representative flow cytometry plots of the mean fluorescence intensities (MFIs) of CD49b and CD49a in liver cNK cells and ILC1s (**D** and **F**), and in NKp46^{+} cells in blood, bone marrow, lung, liver, spleen, and lymph nodes (**E** and **G**) (n=10). (**H** and **I**) Splenocytes from *B2m*$^{-/-}$ and *B2m*$^{+/+}$ were labeled with CFDASE and eF670 respectively. Labeled cells were 1:1 mixed and injected i.v. into *Prdm1*$^{+/+}$ and *Prdm1*$^{\Delta Ncr1}$ recipient mice to evaluate *in vivo* NK cell target-killing ability. Representative flow cytometric plots (left) of transferred cells recovered from recipient mice and percentage (right) of NK cell-specific rejection of donor cells in spleen (n=6) (**H**) and liver (n=7) (**I**) between *Prdm1*$^{+/+}$ and *Prdm1*$^{\Delta Ncr1}$ mice. Data are presented as the mean±SEM and were analyzed by 2-tailed, paired t-test. Differences were evaluated between littermates. Each circle and square on graphs represents an individual mouse; *P*, *P*-value; *, *P*<0.05; **, *P*<0.01, ns, not significant.

Figure 2—figure supplement 1. *Prdm1* affects the IFN-γ secretion ability of type I ILCs.

Representative flow cytometric plot showing the frequency of IFN-γ^{+} cNK cells and ILC1s in spleen and liver between *Prdm1*$^{+/+}$ and *Prdm1*$^{\Delta Ncr1}$ mice (n=5). Liver cells and splenocytes were costimulated in the presence or absence of IL-12 and IL-18 for 12 hours. GolgiStop was added 4 hours before intracellular staining of IFN-γ. Data are presented as the mean±SEM and were analyzed by 2-tailed, paired t-test. Differences were evaluated between littermates. Each circle and square on graphs represents an individual mouse; *P*, *P*-value; *, *P*<0.05; **, *P*<0.01, ns, not significant.

Figure 3—figure supplement 1. *Prdm1* deficiency impairs production of Granzyme B and Perforin in group 1 ILC.

(**A-D**) Representative flow cytometric plot (left) and summary data (right) showing the proportion of GZMB^{+} (**A**) and PRF1^{+} (**D**) splenic cNK cells and relative mean fluorescence intensities (MFIs) of GZMB (**B**) and PRF1 (**C**) in splenic NK cells from *Prdm1*$^{+/+}$ and *Prdm1*$^{\Delta Ncr1}$ mice (n=5). (**E** and **F**)) Representative flow cytometric plots (left) and cumulative data (right) showing the relative MFIs of GZMB (**E**) and PRF1 (**F**) in liver cNK cells and ILC1s from *Prdm1*$^{+/+}$ and *Prdm1*$^{\Delta Ncr1}$ mice (n=5). (**G-I**) Splenic NK cells were divided into different stages according to the expression of maturation markers CD11b and CD27. Representative flow cytometric plot (**G**) and showing the MFIs of GZMB (**H**) and PRF1 (**I**) in evaluated between littermates. Data are presented as the mean±SEM and were analyzed by 2-tailed, paired t-test. Differences were evaluated between littermates. Each circle and square on graphs represents an individual mouse; *P*, *P*-value; r, pearson correlation coefficient; *, *P*<0.05; **, *P*<0.01, ns, not significant.

Figure 4—figure supplement 1. scRNA-seq identified subsets of liver CD45$^+$ cell from *Prdm1*$^{+/+}$ and *Prdm1*$^{\Delta Ncr1}$ mice.

(**A**) Liver CD45$^+$ cells from *Prdm1*$^{+/+}$ and *Prdm1*$^{\Delta Ncr1}$ mice were FACS-sorted for scRNA-seq. (**B**) Quality control of the scRNA-seq data. Violin plot showing the nFeature_RNA, nCount_RNA, and percentage of mitochondrial genes of sequencing cells. nFeature_RNA represents the number of genes detected in each cell, and nCount_RNA represents the total number of molecules detected within a cell. (**C**) Heatmap showing the expression of top 5 upregulated DEGs of each cell cluster by log fold change (computed using Wilcox test in the "FindAllMarkers" function of Seurat, avg_log2FC>0.25; P<0.05). (**D**) Population of twelve liver CD45$^+$ cell clusters between *Prdm1*$^{+/+}$ and *Prdm1*$^{\Delta Ncr1}$ mice. (**E**) Feature plots showing the normalized expression of *Ncr1* (NKp46) and *Klrbc1* (NK1.1) for different cell clusters. (**F**) Dot plot showing the normalized expression of marker genes in liver cNK cells and ILC1s clusters between *Prdm1*$^{+/+}$ and *Prdm1*$^{\Delta Ncr1}$. The dot size represents the percentage of cells expressing selected genes, and color intensity represents the average expression. (**G**) Violin plots showing the expression of marker genes *Itga2* (CD49b), *Itga1* (CD49a), *Eomes, and Tnfsf10* (Trail) between liver cNK cells and ILC1s between *Prdm1*$^{+/+}$ and *Prdm1*$^{\Delta Ncr1}$ mice. (**H**) The percentage of liver cNK cells and ILC1s in liver immune cells between *Prdm1*$^{+/+}$ and *Prdm1*$^{\Delta Ncr1}$.

Figure 4—figure supplement 2. Cluster-specific markers of liver cNK cell clusters.

(**A**) Heatmap showing the expression of top 30 upregulated DEGs by log fold change (computed using Wilcox test in the "FindAllMarkers" function of Seurat, avg_log2FC>0.25; P<0.05), across the three liver cNK cell clusters (*Prf1*^{hi} cNK, *Junb*^{hi} cNK, *Cxcr3*^{hi} cNK) within *Prdm1*$^{+/+}$ and *Prdm1*$^{\Delta Ncr1}$ mice. (**B**) The percentage of *Prf1*^{hi} cNK, *Junb*^{hi} cNK, and *Cxcr3*^{hi} cNK cells in liver immune cells between *Prdm1*$^{+/+}$ and *Prdm1*$^{\Delta Ncr1}$. (**C**) Feature plots showing the normalized expression of selected markers for liver cNK cell populations. (**D**) Violin plots showing the normalized expression of DEGs for each cNK cluster within *Prdm1*$^{+/+}$ and *Prdm1*$^{\Delta Ncr1}$ mice. (**E-G**) GSEA of the enrichment of Mitochondrial protein (**E**), Oxidative phosphorylation (**F**), and Respiratory electron transport chain (**G**) in *Junb*^{hi} cNK cluster compared with clusters of *Prf1*^{hi} and *Cxcr3*^{hi} cNK cells. NES, normalized enrichment score. (**H**) Violin plot showing the ILC1 signature score for different cNK cell clusters, calculated using the signature genes of ILC1 cluster. (**I**) Violin plots showing the normalized expression of cytokine receptor genes (*Il12rb2*, *Il18r1*, and *Il18rap*) for each cNK cluster within *Prdm1*$^{+/+}$ and *Prdm1*$^{\Delta Ncr1}$ mice.

Figure 5—figure supplement 1. Cluster-specific markers of liver ILC1 clusters.

(**A**) Heatmap showing the expression of top 30 upregulated DEGs by log fold change (computed using Wilcox test in the "FindAllMarkers" function of Seurat, avg_log2FC>0.25; P<0.05), across the three ILC1 clusters (*Il7r*^{hi} ILC1, *Klra*^{hi} ILC1, *Gzma*^{hi} ILC1) within *Prdm1*$^{+/+}$ and *Prdm1*$^{\Delta Ncr1}$ mice. (**B**) The percentage of *Il7r*^{hi} ILC1, *Klra*^{hi} ILC1, and *Gzma*^{hi} ILC1 in liver immune cells between *Prdm1*$^{+/+}$ and *Prdm1*$^{\Delta Ncr1}$. (**C**) Feature plots showing the normalized expression of

selected markers for liver ILC1 populations. (**D**) Normalized expression of DEGs for each ILC1 cluster within *Prdm1*$^{+/+}$ and *Prdm1*$^{\Delta Ncr1}$ mice. (**E-G**) GSEA plots (left) depicting the enrichment of NF-kappa B (**E**) , MAPK (**F**), and TNF (**G**) signaling pathways) in *Il7r*^{hi} ILC1 cluster compared with clusters of *Klra*^{hi} and *Gzma*^{hi} ILC1s. Right panel showed dynamic relative expression of the given gene sets from cluster1 to cluster3 between *Prdm1*$^{+/+}$ and *Prdm1*$^{\Delta Ncr1}$. Dots represent the average expression of given gene set in each cell, which was calculated through the sum of normalized expression of each individual gene within the designated gene set in every single cell. NES, normalized enrichment score.

Figure 5—figure supplement 2. Similar and unique gene expression patterns in group 1 ILCs regulated by *Prdm1* and *Hobit*.

(A and **B)** Volcano plots showing the DEGs (avg_log2FC>0.25; P<0.05) in *Prdm1*$^{\Delta Ncr1}$ liver cNK cells (**A**) and ILC1s (**B**) compared to *Prdm1*$^{+/+}$ samples. (**C-F**) *Hobit*^{KO} liver cNK cell and ILC1 clusters were identified from published scRNA-seq data (GES185346 and GSE163452). Volcano plots showing the DEGs (avg_log2FC>0.25; P<0.05) in *Hobit*^{KO} liver cNK cells (**C** and **E**) and ILC1s (**D** and **F**) in comparisons within *Hobit*^{WT} clusters. (**G**) Venn diagram showing the overlapped DEGs within liver cNK cells and in *Prdm1*$^{\Delta Ncr1}$ and *Hobit*^{KO} compared to control samples. (**H**) Selected DEGs common regulated in *Prdm1*$^{\Delta Ncr1}$ and *Hobit*^{KO} liver cNK cells or ILC1s. Upregulated genes (red) and downregulated genes (blue) were indicated. (**I**) Bar plot showing mRNA normalized counts of *Prdm1* in specific NK cell population based on the published bulk RNA-seq data (Flommersfeld et al., GSE180978).

Figure 6—figure supplement 1. Identification of distinct macrophage clusters.

(**A**) Heatmap showing the top 20 upregulated DEGs across four macrophage clusters (computed using Wilcox test in the "FindAllMarkers" function of Seurat, avg_log2FC>0.25; P<0.05). (**B**) Proportions of macrophages (including monocyte-derived macrophages (MDMs) and Kupffer cells (KCs) cluster) in liver immune cells (top, left). Proportions of KCs and MDMs in total macrophages (top, right).The percentage of distinct macrophage clusters in liver total macrophages (bottom, left) and within clusters (bottom, right) between *Prdm1*$^{+/+}$ and *Prdm1*$^{\Delta Ncr1}$. (**C**) Feature plots showing the normalized expression of selected markers for macrophage populations. (**D**) Violin plots showing the expression of selected markers of each macrophage cluster within *Prdm1*$^{+/+}$ and *Prdm1*$^{\Delta Ncr1}$ mice. (**E**) GO analysis of five distinct macrophage clusters. Dot size represents enriched gene number, and color intensity represents significance. (**F**) Representative flow cytometric plots (left) and cumulative data (right) showing the proportions of KCs and MDMs in total liver cells (**G**) Representative flow cytometric plots (left) and cumulative data (right) showing the relative MFIs of Ly6C in liver MDMs. Data are presented as the mean±SEM and were analyzed by 2-tailed, paired t-test. Differences were evaluated between littermates. Each circle and square on graphs represents an individual mouse; *P*, *P*-value; *, *P*<0.05; **, *P*<0.01, ns, not significant.

Figure 6—figure supplement 2. Cell-Cell communication between liver cNK, ILC1s, MDMs, and KCs.

(**A, C, E** and **G**) Circle plots (left) and summary data (right) illustrating the interaction numbers and strength of significant enriched ligand–receptor pairs in cNK-MDMs (**A**), cNK-KCs (**C**), ILC1s-MDMs (**E**), ILC1-KCs (**G**) interactions between *Prdm1*$^{+/+}$ and *Prdm1*$^{\Delta Ncr1}$ cells. The thickness of the line indicates the number of enrich pairs, and the arrow reflects the direction of the interaction. (B, D, F, and H) Bar graphs showing the information flow in selected active signaling patterns in cNK-MDMs (**B**), cNK-KCs (**D**), ILC1s-MDMs (**F**), ILC1-KCs (**H**) interactions between *Prdm1*$^{+/+}$ and *Prdm1*$^{\Delta Ncr1}$ cells. Relative information flow was calculated as the sum of the communication probability in given signaling patterns.

Figure 6—figure supplement 3. Ligand-receptor interaction between type I ILCs and macrophages.

Bubble plots showing the significant ligand-receptor pairs between cNK cells, ILC1s, and macrophages within *Prdm1*$^{+/+}$ and *Prdm1*$^{\Delta Ncr1}$ mice. The highlighted Mif-Cd74 and Cxcl-Cxcr signaling was significantly decreased in *Prdm1*$^{\Delta Ncr1}$ mice. Dot size represents the *P*-value, and color intensity represents the communication probabilities. Empty space indicates a communication probability of zero. *P*-value were calculated by the one-sided permutation test.

Figure 7—figure supplement 1. *Prdm1* maintains the IFN-γ production of liver type 1 ILCs in tumor microenvironment.

(**A**) Representative flow cytometric plot of the frequency of IFN-γ^{+} liver cNK cells and ILC1s from *Prdm1*$^{+/+}$ and *Prdm1*$^{\Delta Ncr1}$ tumor-bearing mice at day 14 after inoculation with B16F10 melanoma cells via intrasplenic injection (n=5). (**B**) reanalysis of statistical significance of IFN-γ production in liver cNK cells and ILC1s after IL-12/IL-18 stimulation (Figure 2F and Figure 7E) using unpaired t-test. Data are presented as the mean±SEM and were analyzed by 2-tailed, paired or unpaired t-test. Differences were evaluated between littermates. Each circle and square on graphs represents an individual mouse; *P*, *P*-value; *, $P<0.05$; **, $P<0.01$, ns, not significant.

Graphical abstract

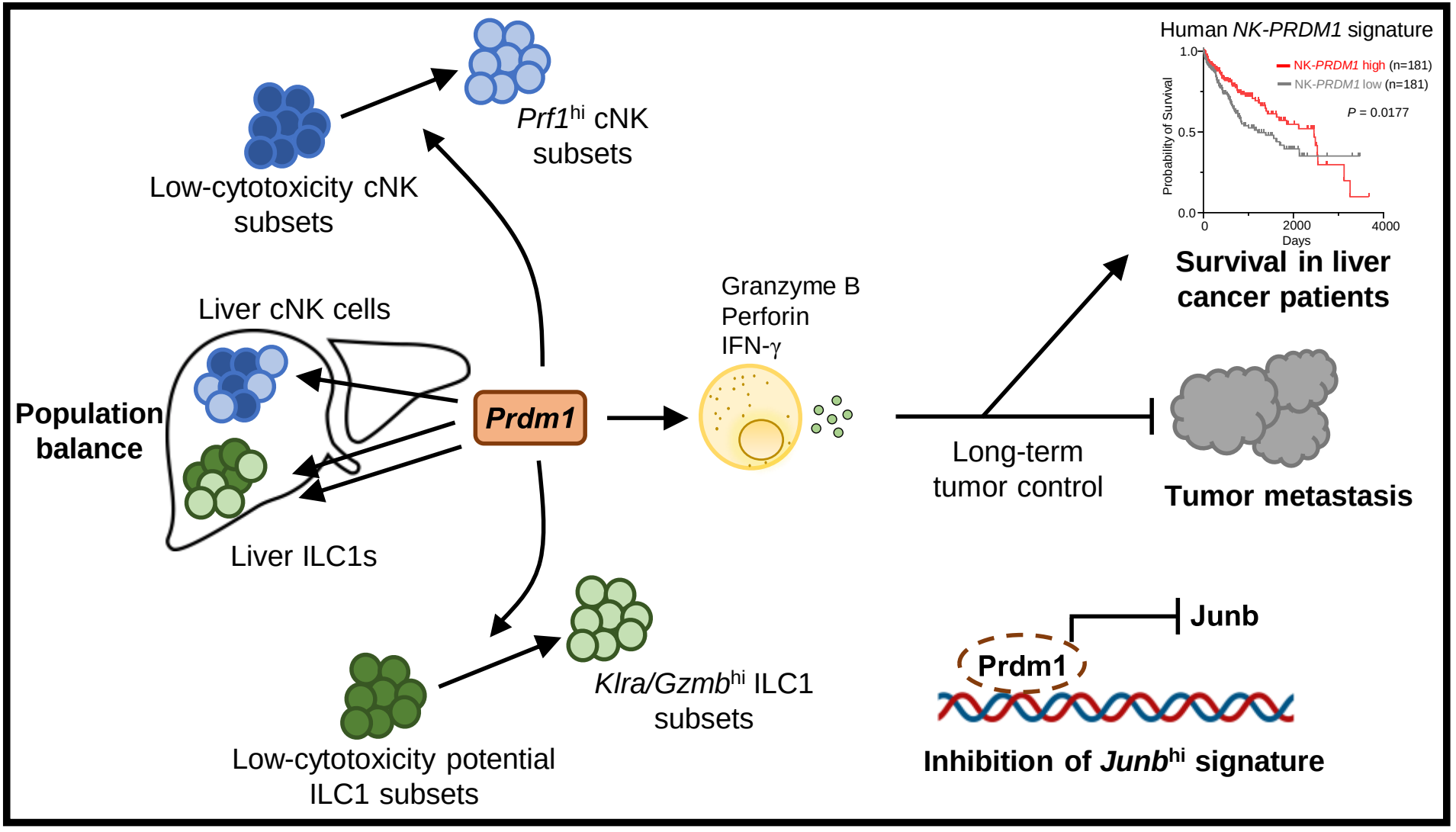

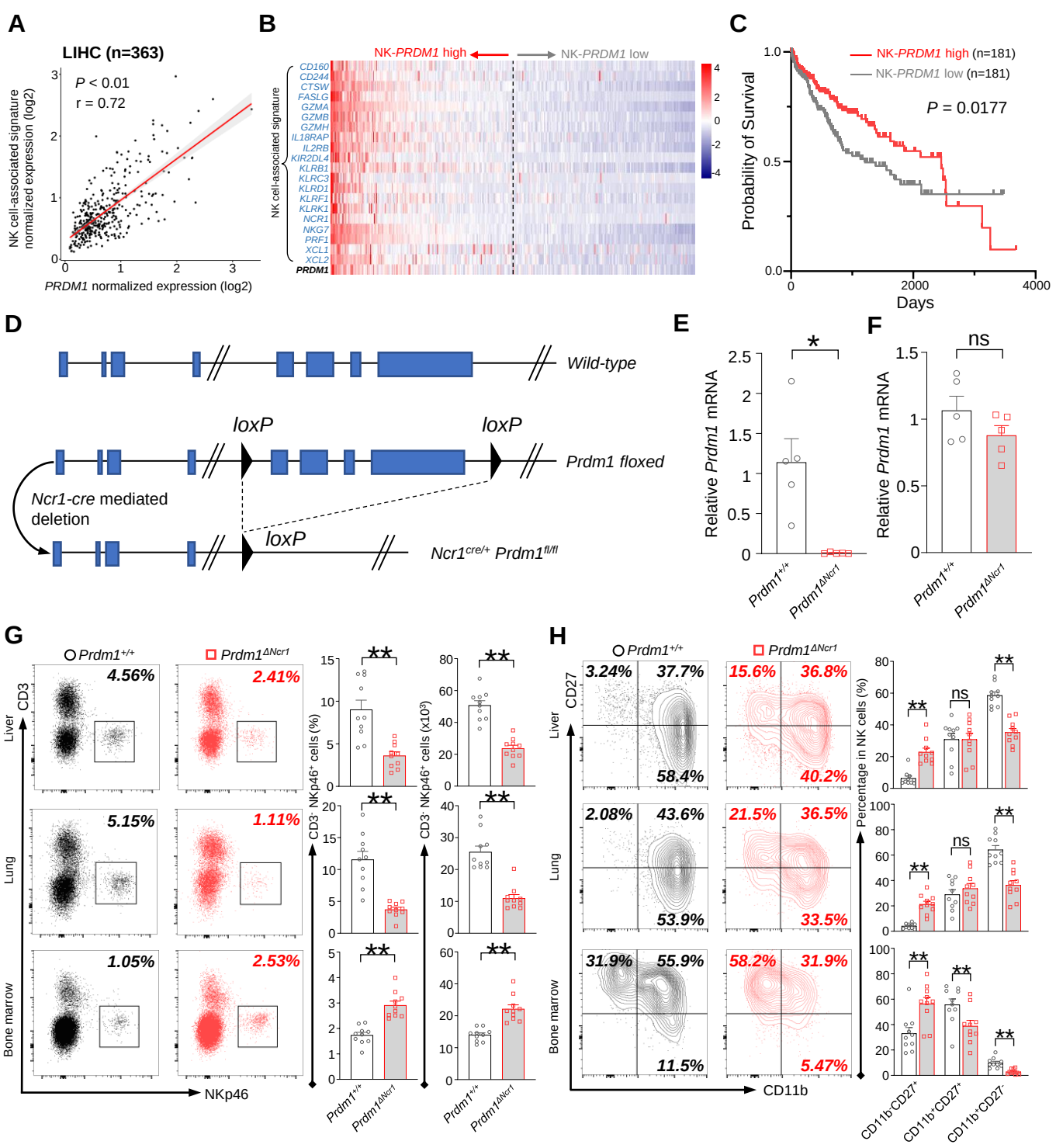
A
LIHC (n=363)
P < 0.01
r = 0.72
NK cell-associated signature normalized expression (log2)
PRDM1 normalized expression (log2)
B
NK-PRDM1 high
NK-PRDM1 low
NK cell-associated signature
CD160
CD244
CTSW
FASLG
GZMA
GZMB
GZMH
IL18RAP
IL2RB
KIR2DL4
KLRB1
KLRC3
KLRD1
KLRF1
KLRK1
NCR1
NKG7
PRF1
XCL1
XCL2
PRDM1
C
NK-PRDM1 high (n=181)
NK-PRDM1 low (n=181)
P = 0.0177
Probability of Survival
Days
D
Wild-type
loxP
loxP
Prdm1 floxed
Ncr1-cre mediated deletion
loxP
Ncr1cre/+ Prdm1fl/fl
E
Relative Prdm1 mRNA
Prdm1+/+
PrdmΔNcr1
F
Relative Prdm1 mRNA
ns
Prdm1+/+
PrdmΔNcr1
G
Prdm1+/+
PrdmΔNcr1
Liver
Lung
Bone marrow
CD3
NKp46
4.56%
2.41%
5.15%
1.11%
1.05%
2.53%
CD3- NKp46+ cells (%)
CD3- NKp46+ cells (x10³)
H
Prdm1+/+
PrdmΔNcr1
Liver
Lung
Bone marrow
CD27
CD11b
3.24%
37.7%
58.4%
15.6%
36.8%
40.2%
2.08%
43.6%
53.9%
21.5%
36.5%
33.5%
31.9%
55.9%
11.5%
58.2%
31.9%
5.47%
Percentage in NK cells (%)
ns
CD11b+CD27+
CD11b-CD27+
CD11b-CD27-

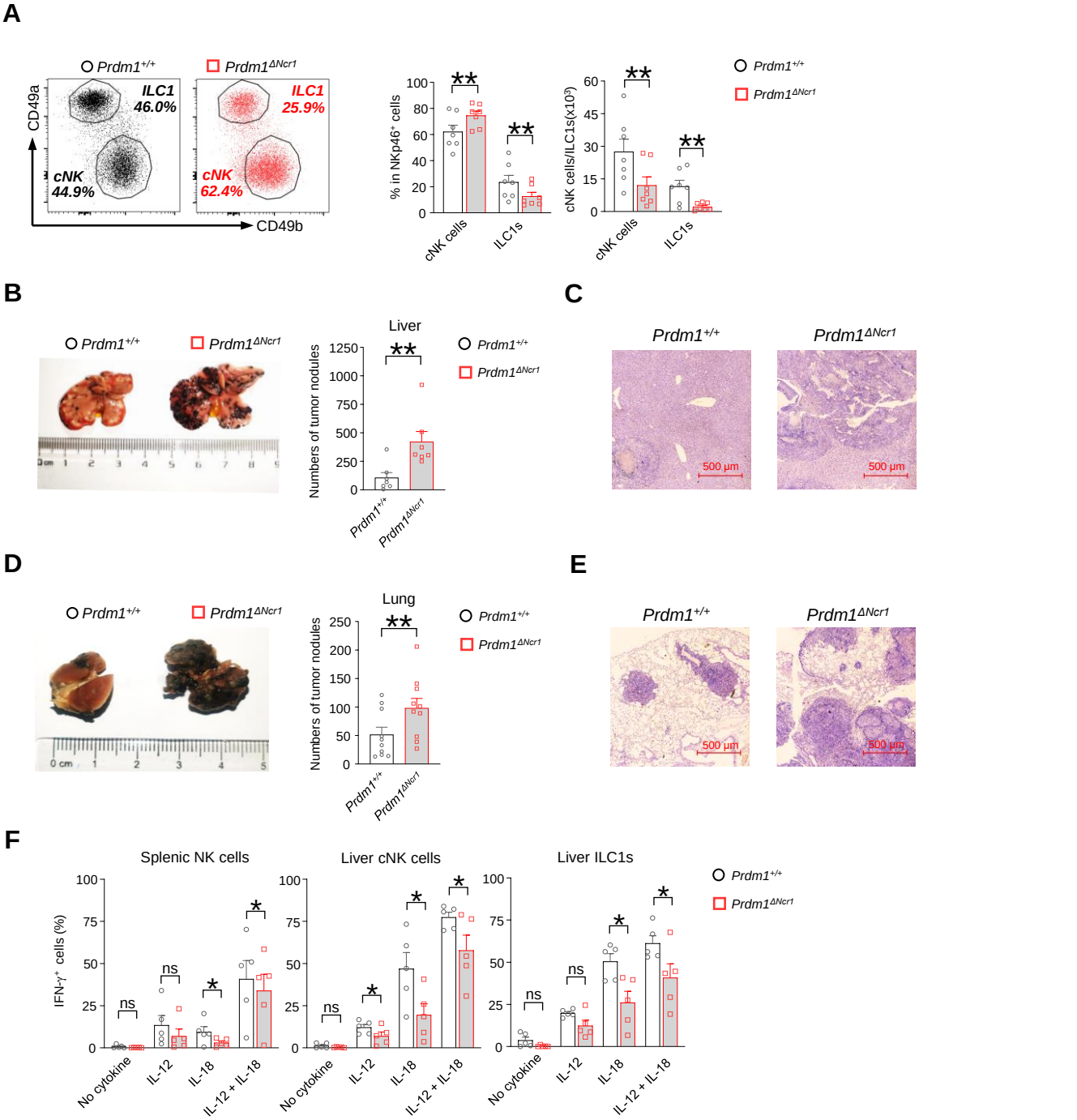
A
Prdm1+/+
Prdm1ΔNcr1
CD49a
CD49b
ILC1
46.0%
cNK
44.9%
ILC1
25.9%
cNK
62.4%
% in NKp46+ cells
cNK cells
ILC1s
cNK cells/ILC1s(x10³)
B
Liver
Numbers of tumor nodules
C
500 μm
D
Lung
E
F
Splenic NK cells
Liver cNK cells
Liver ILC1s
IFN-γ+ cells (%)
ns
No cytokine
IL-12
IL-18
IL-12 + IL-18

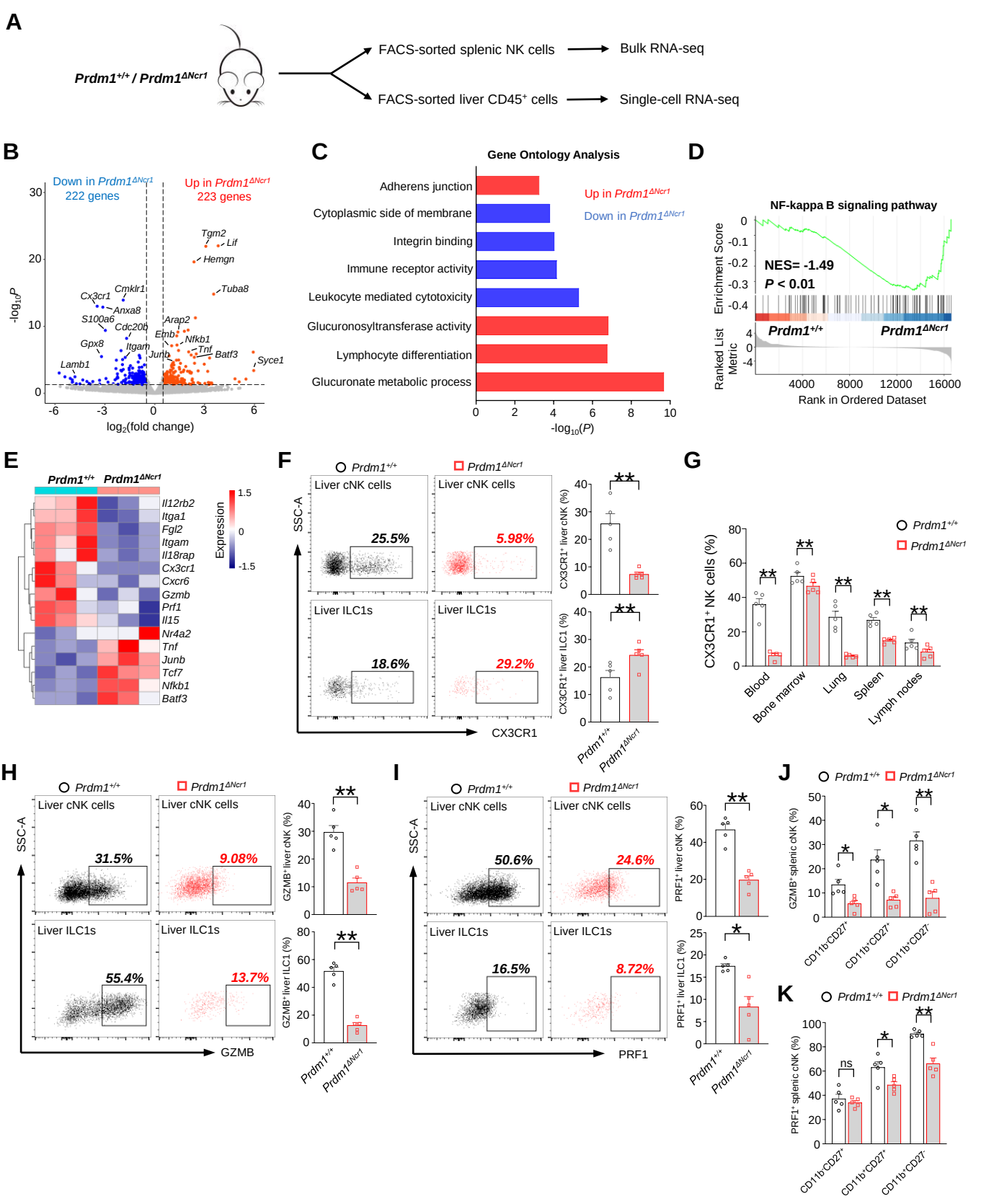
A
Prdm1+/+ / Prdm1ΔNcr1
FACS-sorted splenic NK cells
Bulk RNA-seq
FACS-sorted liver CD45+ cells
Single-cell RNA-seq
B
Down in Prdm1ΔNcr1
222 genes
Up in Prdm1ΔNcr1
223 genes
-log10P
log2(fold change)
Tgm2
Lif
Hemgn
Tuba8
Cx3cr1
Cmklr1
Anxa8
S100a6
Cdc20b
Gpx8
Itgam
Lamb1
Arap2
Emb
Nfkb1
Tnf
Junb
Batf3
Syce1
C
Gene Ontology Analysis
Adherens junction
Cytoplasmic side of membrane
Integrin binding
Immune receptor activity
Leukocyte mediated cytotoxicity
Glucuronosyltransferase activity
Lymphocyte differentiation
Glucuronate metabolic process
Up in Prdm1ΔNcr1
Down in Prdm1ΔNcr1
-log10(P)
D
NF-kappa B signaling pathway
Enrichment Score
NES= -1.49
P < 0.01
Prdm1+/+
Prdm1ΔNcr1
Ranked List Metric
Rank in Ordered Dataset
E
Prdm1+/+
Prdm1ΔNcr1
Expression
Il12rb2
Itga1
Fgl2
Itgam
Il18rap
Cx3cr1
Cxcr6
Gzmb
Prf1
Il15
Nr4a2
Tnf
Junb
Tcf7
Nfkb1
Batf3
F
Prdm1+/+
Prdm1ΔNcr1
Liver cNK cells
Liver ILC1s
SSC-A
CX3CR1
25.5%
5.98%
18.6%
29.2%
CX3CR1+ liver cNK (%)
CX3CR1+ liver ILC1 (%)
G
CX3CR1+ NK cells (%)
Blood
Bone marrow
Lung
Spleen
Lymph nodes
H
Liver cNK cells
Liver ILC1s
GZMB
31.5%
9.08%
55.4%
13.7%
GZMB+ liver cNK (%)
GZMB+ liver ILC1 (%)
I
PRF1
50.6%
24.6%
16.5%
8.72%
PRF1+ liver cNK (%)
PRF1+ liver ILC1 (%)
J
GZMB+ splenic cNK (%)
CD11b-CD27-
CD11b+CD27+
CD11b+CD27-
K
PRF1+ splenic cNK (%)
ns

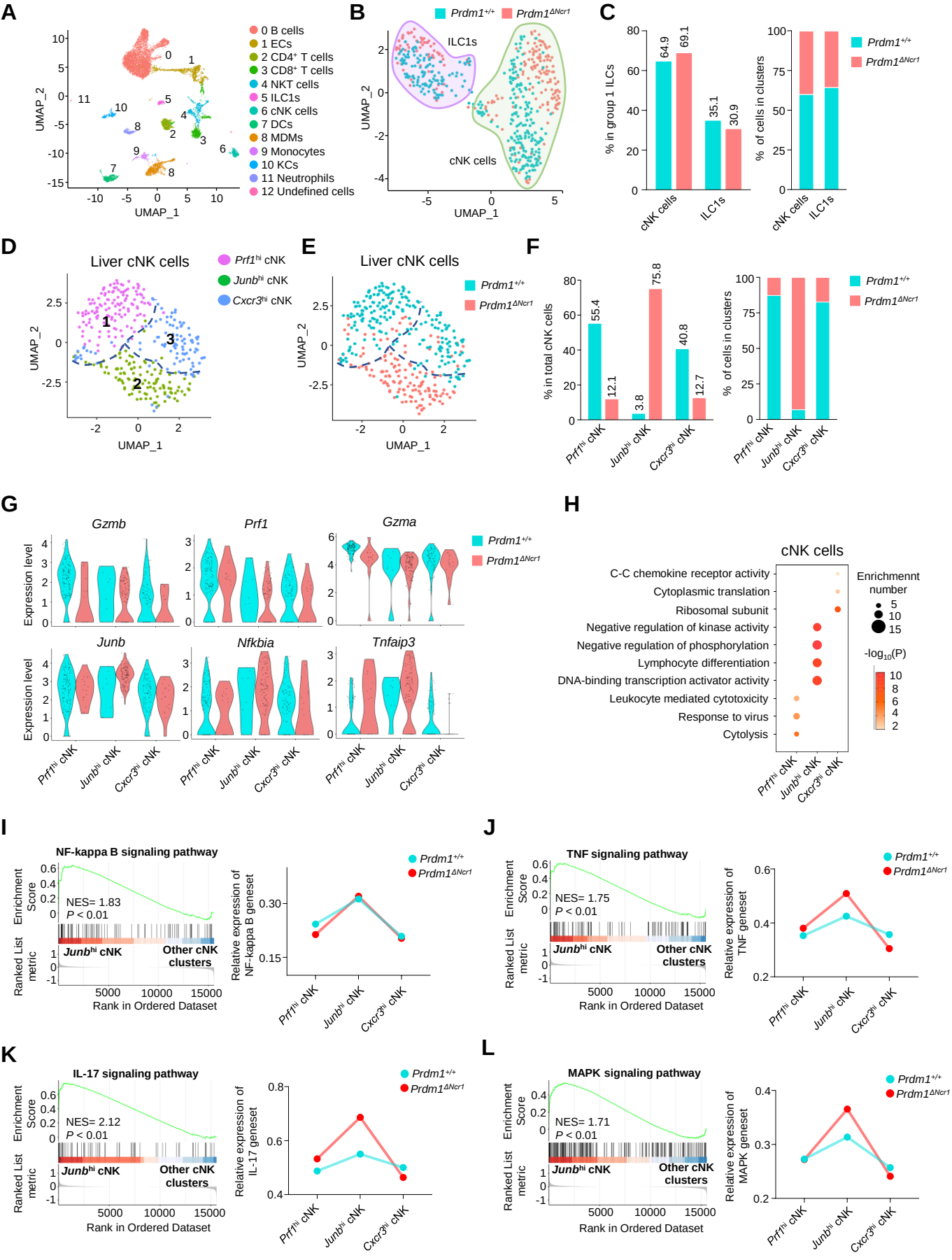
A
0 B cells
1 ECs
2 CD4+ T cells
3 CD8+ T cells
4 NKT cells
5 ILC1s
6 cNK cells
7 DCs
8 MDMs
9 Monocytes
10 KCs
11 Neutrophils
12 Undefined cells
UMAP_1
UMAP_2
B
Prdm1+/+
Prdm1ΔNcr1
ILC1s
cNK cells
C
% in group 1 ILCs
% of cells in clusters
64.9
69.1
35.1
30.9
D
Liver cNK cells
Prf1hi cNK
Junbhi cNK
Cxcr3hi cNK
E
F
% in total cNK cells
55.4
12.1
3.8
75.8
40.8
12.7
G
Gzmb
Prf1
Gzma
Junb
Nfkbia
Tnfaip3
Expression level
H
cNK cells
C-C chemokine receptor activity
Cytoplasmic translation
Ribosomal subunit
Negative regulation of kinase activity
Negative regulation of phosphorylation
Lymphocyte differentiation
DNA-binding transcription activator activity
Leukocyte mediated cytotoxicity
Response to virus
Cytolysis
Enrichmennt number
-log10(P)
I
NF-kappa B signaling pathway
NES= 1.83
P < 0.01
Junbhi cNK
Other cNK clusters
Enrichment Score
Ranked List metric
Rank in Ordered Dataset
Relative expression of NF-kappa B geneset
J
TNF signaling pathway
NES= 1.75
P < 0.01
Relative expression of TNF geneset
K
IL-17 signaling pathway
NES= 2.12
P < 0.01
Relative expression of IL-17 geneset
L
MAPK signaling pathway
NES= 1.71
P < 0.01
Relative expression of MAPK geneset

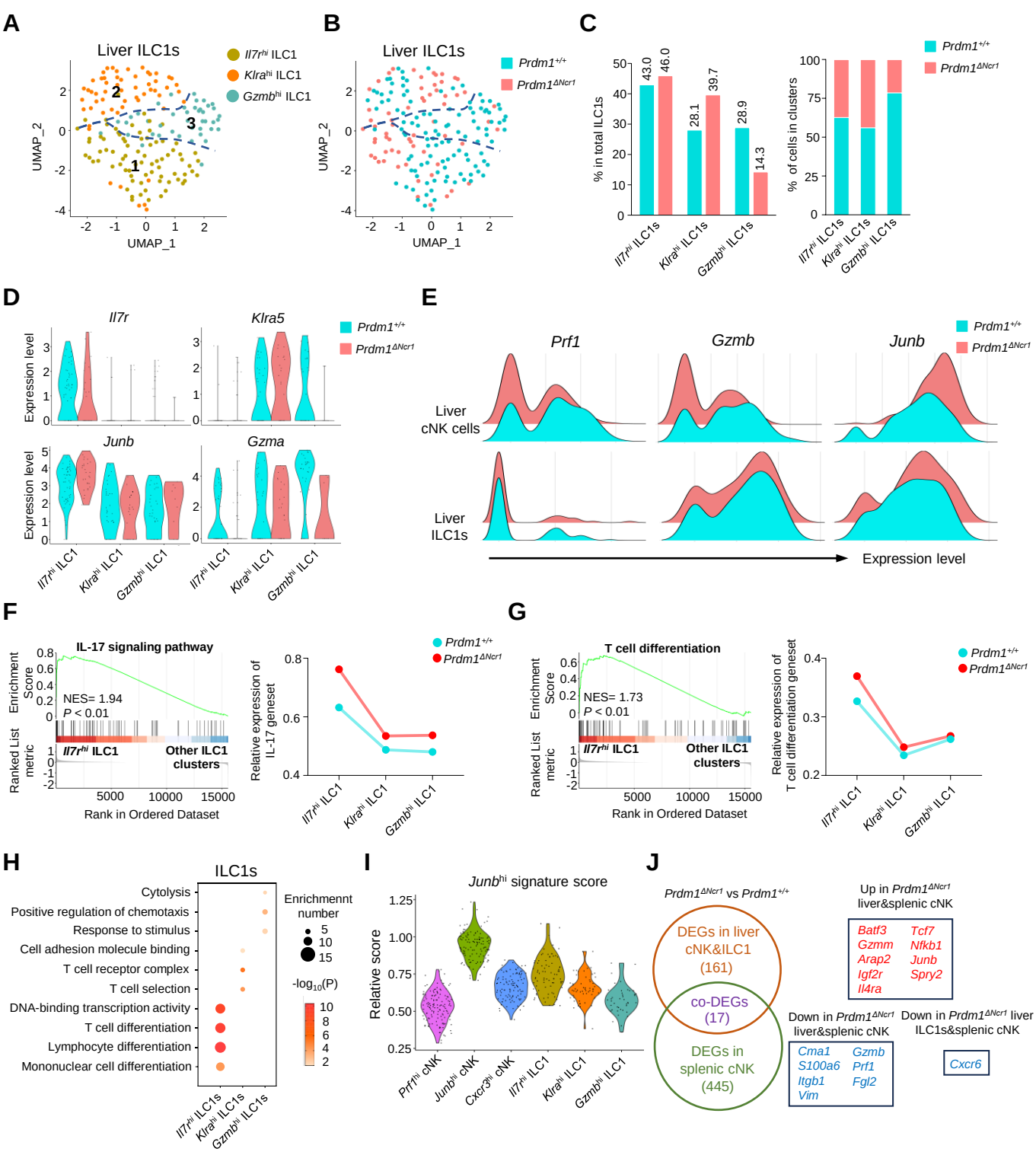
A
Liver ILC1s
Il7r^hi ILC1
Klra^hi ILC1
Gzmb^hi ILC1
UMAP_2
UMAP_1
B
Liver ILC1s
Prdm1^+/+
Prdm1^ΔNcr1
C
% in total ILC1s
% of cells in clusters
43.0
46.0
28.1
39.7
28.9
14.3
D
Il7r
Klra5
Junb
Gzma
Expression level
E
Prf1
Gzmb
Junb
Liver cNK cells
Liver ILC1s
Expression level
F
IL-17 signaling pathway
NES= 1.94
P < 0.01
Enrichment Score
Ranked List metric
Il7r^hi ILC1
Other ILC1 clusters
Rank in Ordered Dataset
Relative expression of IL-17 geneset
G
T cell differentiation
NES= 1.73
P < 0.01
Relative expression of T cell differentiation geneset
H
ILC1s
Cytolysis
Positive regulation of chemotaxis
Response to stimulus
Cell adhesion molecule binding
T cell receptor complex
T cell selection
DNA-binding transcription activity
T cell differentiation
Lymphocyte differentiation
Mononuclear cell differentiation
Enrichmennt number
-log10(P)
I
Junb^hi signature score
Relative score
Prf1^hi cNK
Junb^hi cNK
Cxcr3^hi cNK
Il7r^hi ILC1
Klra^hi ILC1
Gzmb^hi ILC1
J
Prdm1^ΔNcr1 vs Prdm1^+/+
DEGs in liver cNK&ILC1 (161)
co-DEGs (17)
DEGs in splenic cNK (445)
Up in Prdm1^ΔNcr1 liver&splenic cNK
Batf3 Tcf7 Gzmm Nfkb1 Arap2 Junb Igf2r Spry2 Il4ra
Down in Prdm1^ΔNcr1 liver&splenic cNK
Cma1 Gzmb S100a6 Prf1 Itgb1 Fgl2 Vim
Down in Prdm1^ΔNcr1 liver ILC1s&splenic cNK
Cxcr6

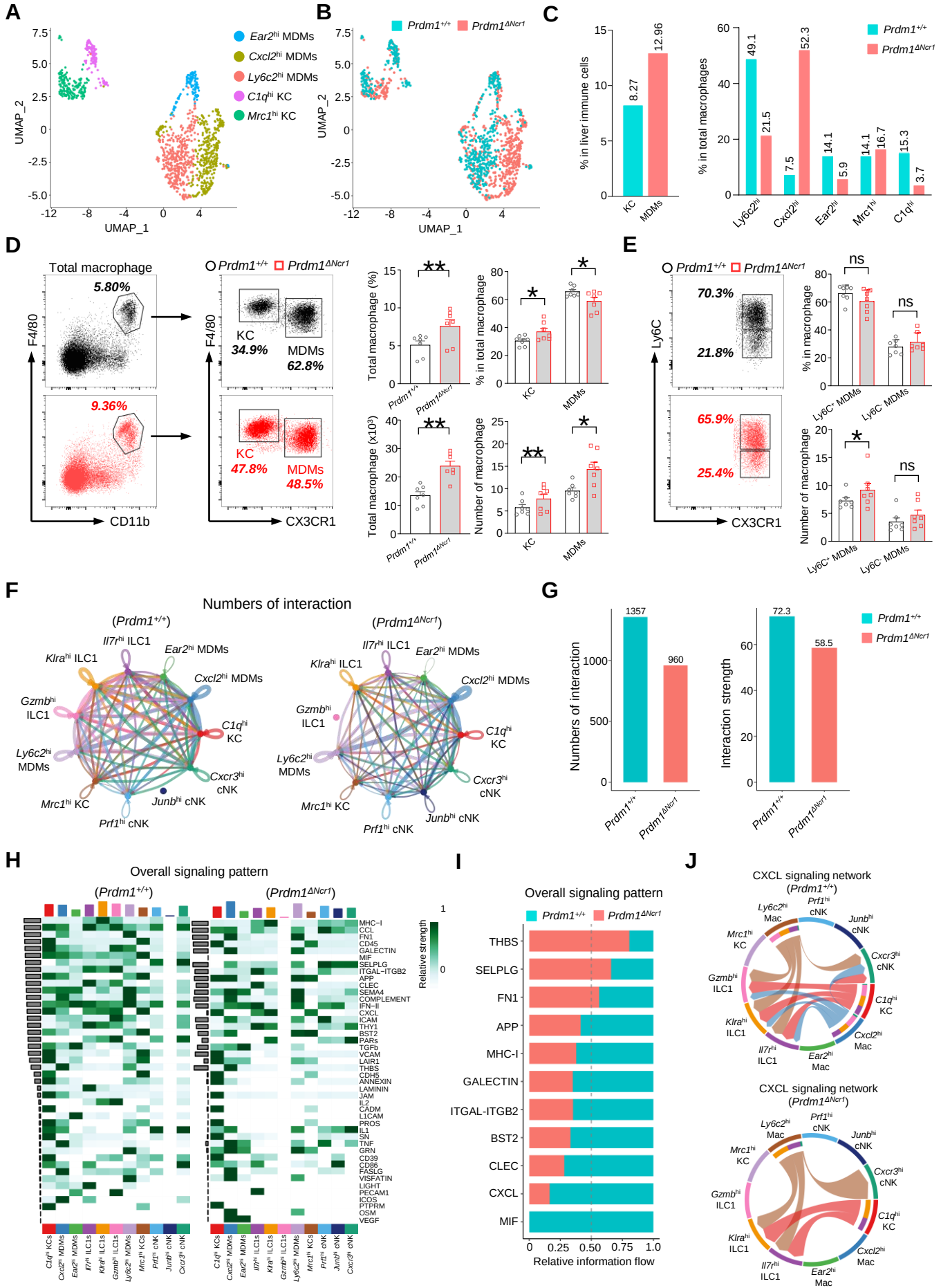
A
Ear2hi MDMs
Cxcl2hi MDMs
Ly6c2hi MDMs
C1qhi KC
Mrc1hi KC
UMAP_2
UMAP_1
B
Prdm1+/+
Prdm1ΔNcr1
C
% in liver immune cells
8.27
12.96
KC
MDMs
% in total macrophages
49.1
21.5
7.5
52.3
14.1
5.9
14.1
16.7
15.3
3.7
Ly6c2hi
Cxcl2hi
Ear2hi
Mrc1hi
C1qhi
D
Total macrophage
5.80%
9.36%
F4/80
CD11b
KC
34.9%
MDMs
62.8%
KC
47.8%
MDMs
48.5%
CX3CR1
Total macrophage (%)
% in total macrophage
Total macrophage (x10³)
Number of macrophage
E
70.3%
21.8%
65.9%
25.4%
Ly6C
CX3CR1
% in macrophage
Number of macrophage
ns
Ly6C+ MDMs
Ly6C- MDMs
F
Numbers of interaction
(Prdm1+/+)
(Prdm1ΔNcr1)
Il7rhi ILC1
Klrahi ILC1
Ear2hi MDMs
Cxcl2hi MDMs
Gzmbhi ILC1
C1qhi KC
Ly6c2hi MDMs
Cxcr3hi cNK
Mrc1hi KC
Junbhi cNK
Prf1hi cNK
G
Numbers of interaction
1357
960
Interaction strength
72.3
58.5
H
Overall signaling pattern
(Prdm1+/+)
(Prdm1ΔNcr1)
Relative strength
MHC-I
CCL
FN1
CD45
GALECTIN
MIF
SELPLG
ITGAL-ITGB2
APP
CLEC
SEMA4
COMPLEMENT
IFN-II
CXCL
ICAM
THY1
BST2
PARs
TGFb
VCAM
LAIR1
THBS
CDH5
ANNEXIN
LAMININ
JAM
IL2
CADM
L1CAM
PROS
IL1
SN
TNF
GRN
CD39
CD86
FASLG
VISFATIN
LIGHT
PECAM1
ICOS
PTPRM
OSM
VEGF
I
Overall signaling pattern
THBS
SELPLG
FN1
APP
MHC-I
GALECTIN
ITGAL-ITGB2
BST2
CLEC
CXCL
MIF
Relative information flow
J
CXCL signaling network
(Prdm1+/+)
(Prdm1ΔNcr1)
Ly6c2hi Mac
Prf1hi cNK
Junbhi cNK
Mrc1hi KC
Cxcr3hi cNK
Gzmbhi ILC1
C1qhi KC
Klrahi ILC1
Cxcl2hi Mac
Il7rhi ILC1
Ear2hi Mac

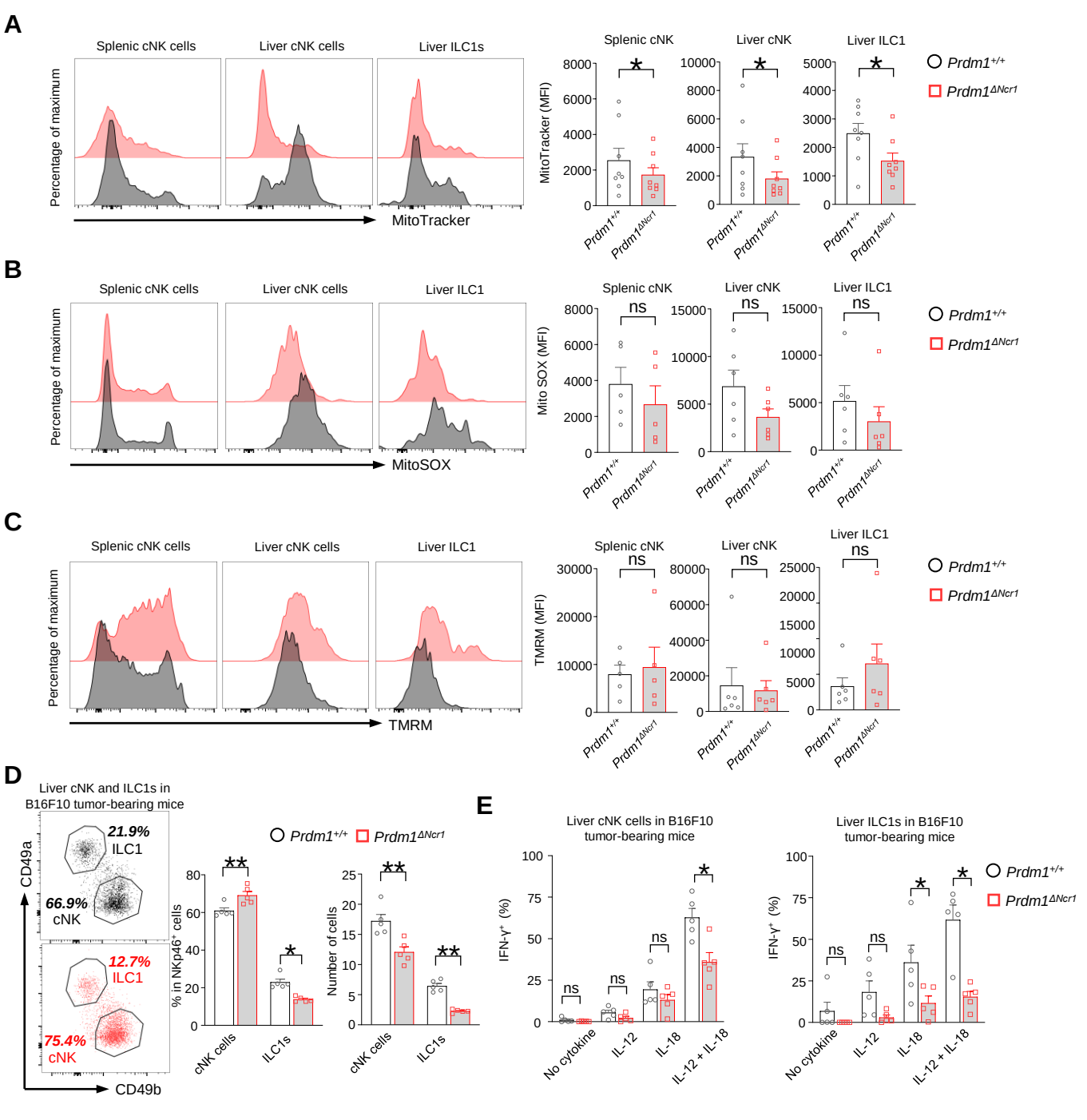
A
Splenic cNK cells
Liver cNK cells
Liver ILC1s
Percentage of maximum
MitoTracker
Splenic cNK
Liver cNK
Liver ILC1
MitoTracker (MFI)
Prdm1+/+
Prdm1ΔNcr1
B
Splenic cNK cells
Liver cNK cells
Liver ILC1
MitoSOX
Mito SOX (MFI)
ns
C
Splenic cNK cells
Liver cNK cells
Liver ILC1
TMRM
TMRM (MFI)
D
Liver cNK and ILC1s in B16F10 tumor-bearing mice
21.9% ILC1
66.9% cNK
12.7% ILC1
75.4% cNK
CD49a
CD49b
% in NKp46+ cells
Number of cells
cNK cells
ILC1s
E
Liver cNK cells in B16F10 tumor-bearing mice
Liver ILC1s in B16F10 tumor-bearing mice
IFN-γ+ (%)
No cytokine
IL-12
IL-18
IL-12 + IL-18